



**UNIVERSIDAD DE INVESTIGACIÓN DE
TECNOLOGÍA EXPERIMENTAL YACHAY**

Escuela de Ciencias Químicas e Ingeniería

**Preparation and Characterization of Crystalline
Nanocellulose Modified as Potential CO₂ Adsorbent.**

Trabajo de integración curricular presentado como requisito para
la obtención del título de Química

Autor:

Hinojosa Peralta Katherine Mishell

Tutor:

MSc. De Lima Eljuri Lola

Ph.D Caetano Sousa Manuel

Urcuquí, Enero 2022

SECRETARÍA GENERAL
(Vicerrectorado Académico/Cancillería)
ESCUELA DE CIENCIAS QUÍMICAS E INGENIERÍA
CARRERA DE QUÍMICA
ACTA DE DEFENSA No. UITEY-CHE-2022-00014-AD

A los 19 días del mes de enero de 2022, a las 15:00 horas, de manera virtual mediante videoconferencia, y ante el Tribunal Calificador, integrado por los docentes:

Presidente Tribunal de Defensa	<u>Dr. OROPEZA OREA, RUTH FIDELINA , Ph.D.</u>
Miembro No Tutor	<u>Dr. NAVAS CÁRDENAS, CARLOS ANDRÉS , Ph.D.</u>
Tutor	<u>Dr. CAETANO SOUSA MANUEL , Ph.D.</u>

El(la) señor(ita) estudiante **HINOJOSA PERALTA, KATHERINE MISHELL**, con cédula de identidad No. **0504076068**, de la **ESCUELA DE CIENCIAS QUÍMICAS E INGENIERÍA**, de la Carrera de **QUÍMICA**, aprobada por el Consejo de Educación Superior (CES), mediante Resolución **RPC-SO-39-No.456-2014**, realiza a través de videoconferencia, la sustentación de su trabajo de titulación denominado: **PREPARATION AND CHARACTERIZATION OF CRYSTALLINE NANOCELLULOSE MODIFIED AS POTENTIAL CO₂ ADSORBENT**, previa a la obtención del título de **QUÍMICO/A**.

El citado trabajo de titulación, fue debidamente aprobado por el(los) docente(s):

Tutor	<u>Dr. CAETANO SOUSA MANUEL , Ph.D.</u>
--------------	---

Y recibió las observaciones de los otros miembros del Tribunal Calificador, las mismas que han sido incorporadas por el(la) estudiante.

Previamente cumplidos los requisitos legales y reglamentarios, el trabajo de titulación fue sustentado por el(la) estudiante y examinado por los miembros del Tribunal Calificador. Escuchada la sustentación del trabajo de titulación a través de videoconferencia, que integró la exposición de el(la) estudiante sobre el contenido de la misma y las preguntas formuladas por los miembros del Tribunal, se califica la sustentación del trabajo de titulación con las siguientes calificaciones:

Tipo	Docente	Calificación
Miembro Tribunal De Defensa	Dr. NAVAS CÁRDENAS, CARLOS ANDRÉS , Ph.D.	10,0
Presidente Tribunal De Defensa	Dr. OROPEZA OREA, RUTH FIDELINA , Ph.D.	10,0
Tutor	Dr. CAETANO SOUSA MANUEL , Ph.D.	9,5

Lo que da un promedio de: **9,8 (Nueve punto Ocho)**, sobre 10 (diez), equivalente a: **APROBADO**

Para constancia de lo actuado, firman los miembros del Tribunal Calificador, el(la) estudiante y el(la) secretario ad-hoc.

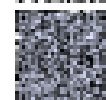
Certifico que en cumplimiento del Decreto Ejecutivo 1017 de 16 de marzo de 2020, la defensa de trabajo de titulación (o examen de grado modalidad teórico práctica) se realizó vía virtual, por lo que las firmas de los miembros del Tribunal de Defensa de Grado, constan en forma digital.

HINOJOSA PERALTA, KATHERINE MISHELL

Estudiante

 **RUTH FIDELINA OROPEZA OREA**
OROPEZA OREA, RUTH FIDELINA , Ph.D.

Presidente Tribunal de Defensa

 **MANUEL CAETANO SOUSA MANUEL , Ph.D.**

Tutor

Dr. NAVAS CÁRDENAS, CARLOS ANDRÉS , Ph.D.
Miembro No Tutor



Escaneo QR para autenticación por
CARLOS ANDRÉS
NAVAS CÁRDENAS

YEPEZ MERLO, MARIELA SOLEDAD
Secretario Ad-hoc



Escaneo QR para autenticación por
MARIELA
SOLEDAD YEPEZ
MERLO

AUTORÍA

Yo, **KATHERINE MISHELL HINOJOSA PERALTA**, con cédula de identidad 050407606-8, declaro que las ideas, juicios, valoraciones, interpretaciones, consultas bibliográficas, definiciones y conceptualizaciones expuestas en el presente trabajo; así como, los procedimientos y herramientas utilizadas en la investigación, son de absoluta responsabilidad de el/la autora (a) del trabajo de integración curricular. Así mismo, me acojo a los reglamentos internos de la Universidad de Investigación de Tecnología Experimental Yachay.

Urcuquí, enero de 2022.



Katherine Mishell Hinojosa Peralta

CI: 050407606-8

AUTORIZACIÓN DE PUBLICACIÓN

Yo, **KATHERINE MISHELL HINOJOSA PERALTA**, con cédula de identidad 050407606-8, cedo a la Universidad de Investigación de Tecnología Experimental Yachay, los derechos de publicación de la presente obra, sin que deba haber un reconocimiento económico por este concepto. Declaro además que el texto del presente trabajo de titulación no podrá ser cedido a ninguna empresa editorial para su publicación u otros fines, sin contar previamente con la autorización escrita de la Universidad.

Asimismo, autorizo a la Universidad que realice la digitalización y publicación de este trabajo de integración curricular en el repositorio virtual, de conformidad a lo dispuesto en el Art. 144 de la Ley Orgánica de Educación Superior

Urcuquí, enero de 2022.



Katherine Mishell Hinojosa Peralta

CI: 050407606-8

DEDICATORIA

Este trabajo se lo dedico a mis padres Franklin y Teresa porque este es el reflejo del esfuerzo y apoyo que siempre he recibido. Este escalón no es solo mío sino suyo también, porque sin ustedes esto no tendría sentido.

También lo dedico a mis hermanos, Alison y Johnny porque han estado conmigo durante este largo camino de altos y bajos, de logros y fallas, pero siempre han estado para apoyarme.

Gracias por ser mi fortaleza en momentos de debilidad y mi inspiración para conseguir mis sueños.

Katherine Hinojosa Peralta

AGRADECIMIENTO

Primero, quiero agradecer a Dios por todo lo que me ha permitido vivir durante esta etapa de mi vida porque todo lo puedo en Cristo que me fortalece. Agradecida por Yachay por las personas que conocí y que ahora representan mucho en mi vida. Especialmente agradezco a mis padres por su apoyo incondicional, su confianza y por creer que en mí más de lo que yo lo hacía. Además, les doy las gracias a mis hermanos, familia, abuelitos y mis padrinos porque cada uno aportó con un granito de arena en mi vida y ahora lo valoro y guardo en el corazón. Agradezco a mi hermana Alison, mi alma gemela quien ha estado a mi lado en todo momento, lista para apoyarme, gracias por todo.

Agradezco a la familia que escogí, mis amigos. Madi, Catherine, Carolina y Belén quienes han estado año tras año apoyándome a pesar de la distancia y ahora celebraremos juntas un logro más. A Kimberly, María Belén y Natasha, mi grupito no fit con quienes he llorado, he reído, he estudiado y hemos ido por choclitos. Son ese grupito que te reinicia la vida después de tanto estrés, gracias por estar siempre. A Alexis quien ha estado conmigo en las buenas, malas y peores. La persona que ha estado para recordarme que todo lo puedo lograr si me lo propongo. Gracias a cada uno de ustedes porque siempre han estado para mí y han hecho cosas que han llenado mi corazón, han estado en esos momentos que solo necesitas un abrazo. La carrera ha sido complicada pero ahora podemos decir que lo logramos, a pesar de todo, lo hicimos y sabemos que las cosas pasan por algo y siempre será para bien!

Agradezco infinitamente a mis profesores tutores Lola y Manuel quienes creyeron y confiaron en mí. Agradezco por la oportunidad que me dieron y por todo el apoyo que he recibido desde el proyecto de mieles hasta ahora con mi tesis que a pesar de las circunstancias logramos cumplir.

Agradezco a la Escuela de Ciencias Física y Nanotecnología en especial al profesor Carlos Reinoso quien me ayudó con el análisis XPS, a la Escuela de Ciencias Biológicas e Ingeniería por haberme facilitado el uso de varios equipos, a la Escuela de Ciencias de la Tierra, Energía y Ambiente en especial a la profesora Elizabeth Mariño quien me ayudó con el análisis SEM/EDS y finalmente a la Escuela de Ciencias Química e Ingeniería por todos mis profesores quienes me enseñaron a amar la ciencia y por el apoyo incondicional.

¡Eternamente Agradecida!

Katherine Hinojosa Peralta

RESUMEN

El cromo es un metal potencialmente tóxico presente en el agua y el agua subterránea debido a factores naturales y antropogénicos. En este estudio, la celulosa cristalina extraída de la cáscara de arroz se modificó para adaptar la estructura y las funcionalidades de la superficie para mejorar su capacidad de adsorción de Cr (VI). Se obtuvo celulosa cristalina (índice de cristalinidad del 72.5%) después de un tratamiento alcalino, y luego se sometió a un proceso de blanqueamiento para eliminar compuestos fenólicos como lignina y hemicelulosa. La celulosa se modificó mediante la adición de grupos amina utilizando polietilenimina (PEI) y glutaraldehído (GA) como reticulante. Se obtuvieron tres diferentes bioadsorbentes funcionalizados y las técnicas de caracterización FTIR-ATR, XRD, SEM-EDS y XPS confirmaron que la celulosa se ha funcionalizado con grupos amina. Se evaluó las capacidades de adsorción y cinética de adsorción, encontrando capacidades de adsorción alrededor de 90 mg g^{-1} , y velocidades de transporte de Cr (VI) desde la fase líquida a la fase sólida en los bioadsorbentes estudiados fueron alrededor de 0.02 s^{-1} , las cuales son lo suficientemente rápidas para sugerir el uso de este adsorbente para el tratamiento de aguas enriquecidas con Cr (VI).

Palabras clave

Cascarilla de arroz, celulosa, bioadsorbentes, polietilenimina (PEI), adsorción, glutaraldehído (GA), modificación.

ABSTRACT

Chromium is a potentially toxic metal present in water and groundwater because of natural and anthropogenic factors. In this study, crystalline cellulose extracted from rice husk, was modified to tailor the structure and surface functionalities to improve its Cr (VI) adsorption capacity. Crystalline cellulose (crystallinity index of 72.5%) was obtained after alkaline treatment, and then it was subjected to a bleaching process to remove phenolic compounds as lignin and hemicellulose. Cellulose was modified by adding amine groups using polyethyleneimine (PEI) and glutaraldehyde (GA) as a crosslinker. Three different functionalized bioadsorbents were obtained, and FTIR-ATR, XRD, SEM-EDS, and XPS characterization techniques confirmed that cellulose has been functionalized with amine groups. Their adsorption capacities and adsorption kinetics were evaluated, finding adsorption capacities about 90 mg g^{-1} , and velocities of Cr (VI) transport from the liquid phase to solid phase in the bioadsorbents studied around 0.02 s^{-1} , which are rapid enough to suggest the use of this adsorbent for the treatment of water enriched with Cr (VI).

Keywords

Rice husk, cellulose, bioadsorbents, polyethyleneimine (PEI), adsorption, glutaraldehyde (GA), modification.

ABBREVIATIONS

CNF: Cellulose Nanofibrils

CNC: Cellulose Nanocrystals

CMF: Carboxymethylated Cellulose Fiber

BC: Bacterial Cellulose

RH: Rice Husk

SA: Silica Aerogels

APTES: (3-Aminopropyl) triethoxysilane

GA: Glutaraldehyde

PEI: Polyethyleneimine

bPEI: Branched PEI

EDC: 1-ethyl-3-(3-dimethylaminopropyl) carbodiimide

FTIR-ATR: Fourier Transform Infrared Spectroscopy - Attenuated Total Reflectance

XRD: X-Ray Diffraction

SEM: Scanning Electron Microscope

EDS: Energy Dispersive Spectroscopy

XPS: X-Ray Photoelectron Spectroscopy

UV-Vis: Ultraviolet-Visible Spectroscopy

K-FCPG: Functionalized Cellulose with bPEI and GA

K-APTES: Modified cellulose with APTES

K-CMC: Carboxymethyl Cellulose

K-CCFCPG: Carboxymethyl Cellulose was Functionalized with bPEI and GA

K-AFCPG: Modified cellulose with APTES and Functionalized with bPEI and GA

K-PGG: Functionalized Cellulose with bPEI and GA (drop by drop)

K-AGG: Modified cellulose with APTES and Functionalized with bPEI and GA (drop by drop)

CrI: Crystallinity Index

TABLE OF CONTENTS

CHAPTER I	1
1. Introduction – Justification	1
1.1. Biadsorbents	2
1.2. Cellulose	2
1.3. Cellulose from Biomass	4
2. Problem Statement	6
3. Objectives	6
3.1. General Objective	6
3.2. Specific Objectives	6
CHAPTER II	7
4. Theoretical Background	7
4.1. Cellulose Surface-Modified	7
4.2. Adsorption Kinetic Models	10
4.2.1. Adsorption Reaction Models	10
4.3. Experimental Characterization Techniques	12
4.3.1. Fourier Transform Infrared Spectroscopy (FTIR)	12
4.3.2. X-Ray Diffraction (XRD)	12
4.3.3. Scanning Electron Microscopy (SEM)	12
4.3.4. Ultraviolet-Visible Spectroscopy (UV-Vis)	13
4.3.5. X-Ray Photoelectron Spectroscopy (XPS)	13
CHAPTER III	14
5. Methodology	14
5.1. Materials, Reagents and Equipment	14
5.2. Extraction and Purification of Cellulose from Rice Husk	15
5.2.1. Removal of Impurities: Alkaline Treatment	15
5.2.2. Purification of Crude Cellulose: Cellulose Bleaching	15

5.3. Preparation of Bioadsorbents	16
5.3.1. Synthesis Functionalized Cellulose with bPEI (K-FCPG).....	16
5.3.2. Synthesis of APTES Modified Cellulose (K-APTES).....	17
5.3.3. Synthesis of Carboxymethyl Cellulose (K-CMC) and Functionalized with bPEI (K-CCFCPG).....	18
5.3.4. Synthesis Functionalized Cellulose with bPEI (K-AFCPG).....	19
5.4. Design of Adsorption Experiments.....	20
5.4.1. Kinetic Batch Studies on Cr (VI) Adsorption.....	20
5.4.2. Data Analysis of Adsorption Kinetics.....	21
5.5. Characterization Techniques.....	23
5.5.1. Fourier Transform Infrared Spectroscopy- Attenuated Total Reflectance (FTIR-ATR).....	23
5.5.2. X-Ray Diffraction (XRD).....	23
5.5.3. Scanning Electron Microscopy/Energy Dispersive X-Ray Spectrometer (SEM/EDS).....	23
5.5.4. Ultraviolet- Visible Spectroscopy (UV-Vis).....	24
5.5.5. X-Ray Photoelectron Spectroscopy (XPS).....	24
CHAPTER IV	25
6. Results and Discussion.....	25
6.1. Extraction and Characterization of Cellulose from Rice Husk.....	25
6.1.1. FTIR–ATR Analysis.....	26
6.1.2. XRD Analysis.....	27
6.2. Synthesis Results.....	28
6.3. FTIR-ATR Analysis.....	31
6.3.1. K-FCPG Bioadsorbent.....	31
6.3.2. K-APTES Bioadsorbent.....	33
6.3.3. K-CCFCPG Bioadsorbent.....	34
6.3.4. K-AFCPG Bioadsorbent.....	34

6.4. SEM-EDS Analysis	36
6.5. Adsorption Kinetics	38
6.5.1. Kinetic Batch Studies on Cr (VI) Adsorption	38
6.5.2. Cr (VI) Adsorption Kinetics of K-FCPG and K-AFCPG	40
6.6. Chromium Adsorption	43
6.6.1. FTIR-ATR Analysis	43
6.6.2. XPS Analysis	45
6.7. Proposals for Reactions of the Synthesis of Bioadsorbents Cellulose Base	
48	
CHAPTER V	51
7. Conclusions	51
8. Recommendations	52
9. References	53

LIST OF FIGURES

Figure 1. Cellulose.....	3
Figure 2. Different chemical functionalization of cellulose ⁴³	7
Figure 3. Cross-linking cellulose–PEI in the presence of (A) GA and (B) EPI ⁴³	8
Figure 4. Preparation of cellulose–PEI xerogel scaffolds ⁴³	9
Figure 5. Schematic of the process of mass transfer during adsorption ⁴⁴	10
Figure 6. (A) Rice Husk, (B) Sieve, (C) Ground RH	15
Figure 7. Schematic illustration of the synthesis of K-FCPG	16
Figure 8. (A) Schematic illustration of the synthesis of K-APTES.....	17
Figure 9. Schematic illustration of the synthesis of K-CMC and K-CCFCPG	18
Figure 10. Schematic illustration of the synthesis of K-AFCPG.....	19
Figure 11. (A) RH after alkaline treatment, (B) RH after bleaching process, (C) Bleached Cellulose: crushed RH, and (D) Bleached Cellulose: RH powder	25
Figure 12. FTIR–ATR spectrum of (A) cellulose of crushed RH, and (B) cellulose of RH powder.....	26
Figure 13. X-ray Diffraction pattern of cellulose	27
Figure 14. K-FCPG2 bioadsorbent	30
Figure 15. (A) K-PGG bioadsorbent, (B) K-AGG bioadsorbent, and (C) Comparison between two methods of add GA	31
Figure 16. FTIR–ATR spectrum of (A) K-FCPG bioadsorbent and (B) K-FCPG2 bioadsorbent.....	32
Figure 17. FTIR-ATR spectrum of K-APTES	33
Figure 18. FTIR-ATR spectra (A) K-CMC bioadsorbent and (B) K-CCFCPG bioadsorbent.....	34
Figure 19. FTIR–ATR spectra (A) K-APTES (B) K-FCPG bioadsorbent and (C) K-AFCPG bioadsorbent.....	35
Figure 20. (A) SEM/EDS and (B) map of K-CCFCPG.....	37
Figure 21. (A) SEM/EDS and (B) map of K-FCPG	37
Figure 22. (A) SEM/EDS and (B) map of K-AFCPG	37
Figure 23. Cr Removal (%) of Cr (VI) (A) 5 mg and (B) 20 mg of K-FCPG and K-AFCPG	39
Figure 24. Cr (VI) adsorption kinetics for 100 ppm solutions in contact with 5 mg of (A) K-AFCPG and (B) K-FCPG material.....	40

Figure 25. Cr (VI) adsorption kinetics for 100 ppm solutions in contact with 5 mg of A) K-AFCPG, and B) K-FCPG material and best fits to data were successfully obtained assuming pseudo first-order and non-linear fits	41
Figure 26. Isotherm for K-AFCPG	42
Figure 27. Adsorption mechanisms	42
Figure 28. FTIR–ATR spectra of a) K-FCPG bioadsorbent b) K-FCPG loaded of Cr (VI)	43
Figure 29. FTIR–ATR spectra of a) K-AFCPG bioadsorbent b) K-AFCPG loaded of Cr (VI)	44
Figure 30. FTIR–ATR spectra of a) K-FCPG loaded of Cr (VI) b) K-AFCPG loaded of Cr (VI)	44
Figure 31. (A) K-FCPG and (B) K-AFCPG after adsorption of Cr (VI)	45
Figure 32. Cr 2p XPS spectrum of (A) K-FCPG and (B) K-AFCPG.....	46
Figure 33. N1s XPS spectrum of (A) K-FCPG and (B) K-AFCPG	47
Figure 34. K-FCPG Reaction	48
Figure 35. K-APTES reaction (a) Synthesis of Silanol and (b) Silanol and cellulose reaction	49
Figure 36. K-AFCPG Reaction.....	50

LIST OF TABLES

Table 1. Rice Husk Composition	5
Table 2. Reagents.....	14
Table 3. Specific weight used for the batch experiment.....	20
Table 4. Kinetics Models	21
Table 5. Synthesis of bioadsorbents results	28
Table 6. Percentage of Cr (VI) adsorption with different weights of bioadsorbents.....	38
Table 7. Kinetic parameters	41

CHAPTER I

1. Introduction – Justification

Water pollution has become a major source of concern and a priority for researchers in the last few years due to water quality being closely related to human health.¹ Some causes of water pollution are industrial wastes, mining activities, sewage, pesticides, chemical fertilizers, energy use, radioactive waste, and heavy metals.² Heavy metals can be emitted into the environment by natural and anthropogenic causes. The significant anthropogenic sources are mining operations, electroplating, metallurgy, chemical plants, agriculture, etc. For that, heavy metals are considered one of the most important polluting, especially for developing countries.³ Some heavy metals have bio-importance as trace elements. However, the biotoxic effects in human biochemistry are of concern principally for the ingestion through contaminated marine animals. High concentrations are known to produce a range of toxic effects as encephalopathy, cognitive impairment, behavioral disturbances, kidney damage, anemia, and toxicity to the reproductive system.⁴

Also, heavy metals are persistent environmental contaminants since they cannot be degraded or destroyed. Some of the most important are: Pb, Cd, Zn, Hg, As, Ag, Cr, Cu, and Fe.⁵ Pb, Cr, and Cd are highly toxic that can negatively affect the environment and living beings. Cr (VI) is a priority pollutant that can penetrate the cell wall, and it is genetically toxic, mutagenic, and carcinogenic.⁶ The forms of chromium that most commonly occur in natural waters are trivalent chromium Cr (III) and hexavalent chromium Cr (VI). Additionally, the Cr (VI) exists mainly as chromate ion (CrO_4^{2-}), dichromate ion ($\text{Cr}_2\text{O}_7^{2-}$), hydrogen chromate ion (HCrO_4^-), and chromic acid (H_2CrO_4), depending on the Cr concentration and pH in solution. Cr (VI) is considered much more toxic than Cr (III) when it exists as CrO_4^{2-} , HCrO_4^- , and $\text{Cr}_2\text{O}_7^{2-}$ due to having higher solubility and mobility.⁷

According to the World Health Organization (WHO), the maximum allowable limit for chromium in drinking water is 0.05 mg/ L.⁸ However, in 2020, analyzed the quality of water in three cities of Ecuador, Quito, Ibarra, Guayaquil, through the heavy metal pollution index (HPI) analysis. The studies determined the presence of heavy metals in

surface waters, sediments, fish, soils, and crops.⁴ Also, the showed that water sources in Guayaquil have Pb and Cr above WHO recommended values.⁹

The technologies most used to treat Cr (VI) are chemical precipitation, reverse osmosis, ion exchange, extraction, and adsorption¹⁰. Adsorption has been considered the most promising option due to its advantages. The most common adsorbents are activated carbon, inorganic materials, and natural materials or wastes. During the last years, adsorbents produced from natural materials have extensive attention because of their high efficiency and low cost to Cr (VI) adsorption.

1.1. Biadsorbents

Adsorption is the most promising technology for water-contaminated treatment due to its high efficiency, ease of operation, and economic advantages. The greatest advantage of the adsorption method is that by-products, such as sludge, are not generated. To select a better adsorbent for removing water contaminants depends on concentration, type of pollutant, and efficiency for the pollutant.¹¹ Therefore, in the last years, some adsorbents have been developed, such as activated carbon, nanoparticles, zeolite, clay, ion exchangers, bark, biomass, lignin, metal-organic frameworks, and polymers.

The worrying environmental impact has generated great interest in developing engineering products based on natural resources. The natural polymers are effective bio-adsorbent for the removal of various dyes and heavy metals because they are biodegradable, low-cost, and non-toxic, making them a potential material.¹² The use of cellulose has been highlighted as one of the most abundant sources among natural polymers.

1.2. Cellulose

Cellulose is renewable polysaccharide, biodegradable, inexpensive, and the most abundant on earth. Cellulose $(C_6H_{10}O_5)_n$ is a linear polysaccharide composed of repeating units, which chemical structure can be seen in Figure 1. Also, its comprised of two anhydro glucose rings linked by oxygen in covalently bonded to C₁ of one glucose ring and C₄ of the adjoining ring so-called β (1 \rightarrow 4) glycosidic bonds.¹³ Cellulose can be synthesized by microorganisms or can be extracted from a different natural sources.¹⁴ The natural source include cotton, hardwoods and softwoods, flax, hemp, jute, ramie, grasses, bagasse, bamboo, rice husk, sugar beet, wood pulp, bacteria, rice straw and algae biomass.

¹⁵⁻¹⁸. Cellulose serves as a structural material within the plant cell walls with variation in its content. It can be since 40 % to 90 % how is in the case of cotton seed hairs that is considered as a pure source with 90.9 % cellulose content.¹⁵

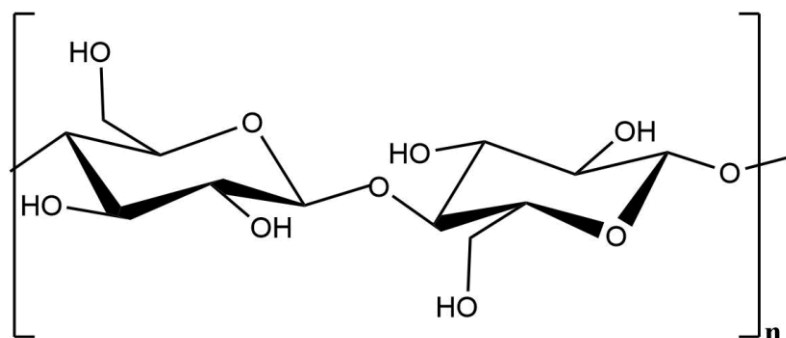


Figure 1. Cellulose

From cellulose can obtain cellulose nanofibrils (CNF), cellulose nanocrystals (CNC), and bacterial cellulose (BC) have different production and morphology.

CNF are three-dimensional networks formed from the assembly of glucose molecules through Van der Waals interactions. Furthermore, CNF can be produced through some techniques such as electrospinning, refining, homogenization, grinding, cryocrushing, ultrasonication, and steam explosion.¹⁹ These cellulose chains are consist of two regions: one region is highly ordered structure/crystalline and the other region is disordered/amorphous. The crystalline region extracted from cellulose microfibrils resulting in cellulose nanocrystals (CNC).²⁰

CNC combine important cellulose properties, such as hydrophilicity, high surface area, crystalline character, excellent mechanical, tensile strength and high degree of modification.²¹ CNCs are obtained via strong acid hydrolysis and can provide low-cost, sustainable, and eco-friendly materials for various applications.

Bacterial cellulose (BC) or microbial cellulose is obtained from certain bacteria via an approach involving enzymatic polymerization of glucose. BC is composed of nano-sized fibrils of around 20–100 nm diameter. BC is characterized by a high water-holding capacity due to being very hydrophilic, high degree of crystallinity, and is free from lignin and hemicellulose.^{22,23}

1.3. Cellulose from Biomass

Rice is the priority food of the agribusiness, and it is food consumed by approximately half of the seven billion inhabitants of the world, for which a large amount of waste is generated.²⁴ Rice activity can reach a world production of 670 million tons of rice, of which 91 % is harvested in Asia, 5 % in America, 3% in Africa and the remaining 1 % in Europe.²⁵ In 2019, Ecuador production was 1.099.686 tonnes,²⁶ which represents 30.8 %²⁷ of the total area sowed. Rice husk (RH) is a by-product of industrial processing and represents 25 wt%.

Rice farmers contribute at the environmental contamination due to they collect the natural waste to dispose of it by burning it in the open air or throwing it into lakes or rivers. In the case of rice waste, burning the rice husk generates dust that contributes to the greenhouse effect.²⁸ The ashes from RH are rich in silicon with levels of 64.5 % that directly affect humans. Also, the high levels cause gastric problems and later kidney stones.²⁹

Rice husk composition (Table 1) allow to know some applications such as the synthesis of zeolitic materials, oxide-free ceramics, silica aerogels (SA), and mesoporous carbon. It can be practical solutions to mitigate the contamination by rice waste. However the most viable solution is using RH as a cellulose source due to its high content.³⁰ The cellulose obtained from RH has several advantages since it is abundant, non-toxic, resistant, and chemical treatments can modify the surface to improve specific properties.³¹ Also, depending on the chemical treatment, it may have selectivity for particular applications. RH as a source of cellulose acquires added value and mitigates the impact of agro-industrial waste.

Table 1. Rice Husk Composition

Composition	Percentage	Reference
Cellulose	28.6 % - 41.5 %	6,25
Hemicellulose	14 % - 28.6 %	25,28
Lignin	20.4 % - 33.7 %	6,25,30,31
Silica	15 % - 20 %	6,28
Proteins	2.0 % - 2.8 %	32
Fats	0.3 % - 0.8 %	31
Crude fiber	34.5 % - 45.9 %	31
Moisture	10 % - 15 %	6
C	30 % - 50.5 %	25
H	4.4 % - 6.6 %	25
O	35.2 % - 59.5 %	25
N	0.05 % - 4.3 %	25
S	0.0 % - 0.6 %	25

In this work, cellulose was extracted from the rice husk through chemical treatment. The cellulose was modified and functionalized by PEI and GA like cross-linking. Three bioadsorbents were synthesized using different modification processes to later be functionalized. Bioadsorbents were characterized by FTIR-ATR, XRD, SEM, EDS, and XPS. In addition, the adsorption capacity of the bioadsorbents was determined using and UV-Vis spectroscopy. Finally, the adsorption kinetics were evaluated in the bioadsorbents that have the highest adsorption capacity of Cr (VI) in water.

2. Problem Statement

In the last years, Cr (VI) levels have increased in the water due to sources of anthropogenic origin such as metalliferous mining, agricultural materials, waste disposal landfill leachate, electronics, paints, and pigments.³³ Water pollution is a serious issue because it directly affects the well-being of living beings. According to studies carried out in Ecuador, results determined that the presence of Cr (VI) in human biochemistry has resulted from ingestion of food contaminated with this heavy metal. The use of cellulose-based adsorbents has shown advantages over technologies for the treatment of Cr (VI). That is why this work evaluates the capacity of a new adsorbent material proposal for treating Cr (VI) based on natural resources to improve the efficiency of conventional adsorbents. Also, the rice husk is a waste of rice industry that is burned or disposed of in rivers causing a serious damage to the environment.

3. Objectives

3.1. General Objective

To prepare and characterize crystalline cellulose modified from rice husk for the adsorption of Cr (VI) present in water.

3.2. Specific Objectives

- To obtain crystalline cellulose from rice husk through alkaline treatment and a bleaching process.
- To prepare bioadsorbents from cellulose obtained to give value to the biomass.
- To functionalize the cellulose surface through the addition of amino groups by PEI.
- To test and characterize several modification methods based on the cellulose obtained to evaluate the adsorption capacity.
- To determine the best bioadsorbent proposal for the removal of Cr (VI) in water.

CHAPTER II

4. Theoretical Background

4.1. Cellulose Surface-Modified

Nowadays, the impact of water pollution has generated the development of new materials and techniques for the treatment of heavy metals e.g. (Pb, Cd, Zn, Hg, As, Ag, Cr, Cu, Fe)⁵. Adsorbents produced from biomass, especially cellulose base biomaterials are the most used because of their excellent physical, chemical, and mechanical properties. However, the cellulose surface requires chemical modifications to improve the adsorption capacity and physicochemical properties. The treatments for the modification of cellulose are esterification, etherification, halogenation, amidation, carboxymethylation, oxidation, sulphonation, phosphorylation and silylation (Figure 2).³⁴

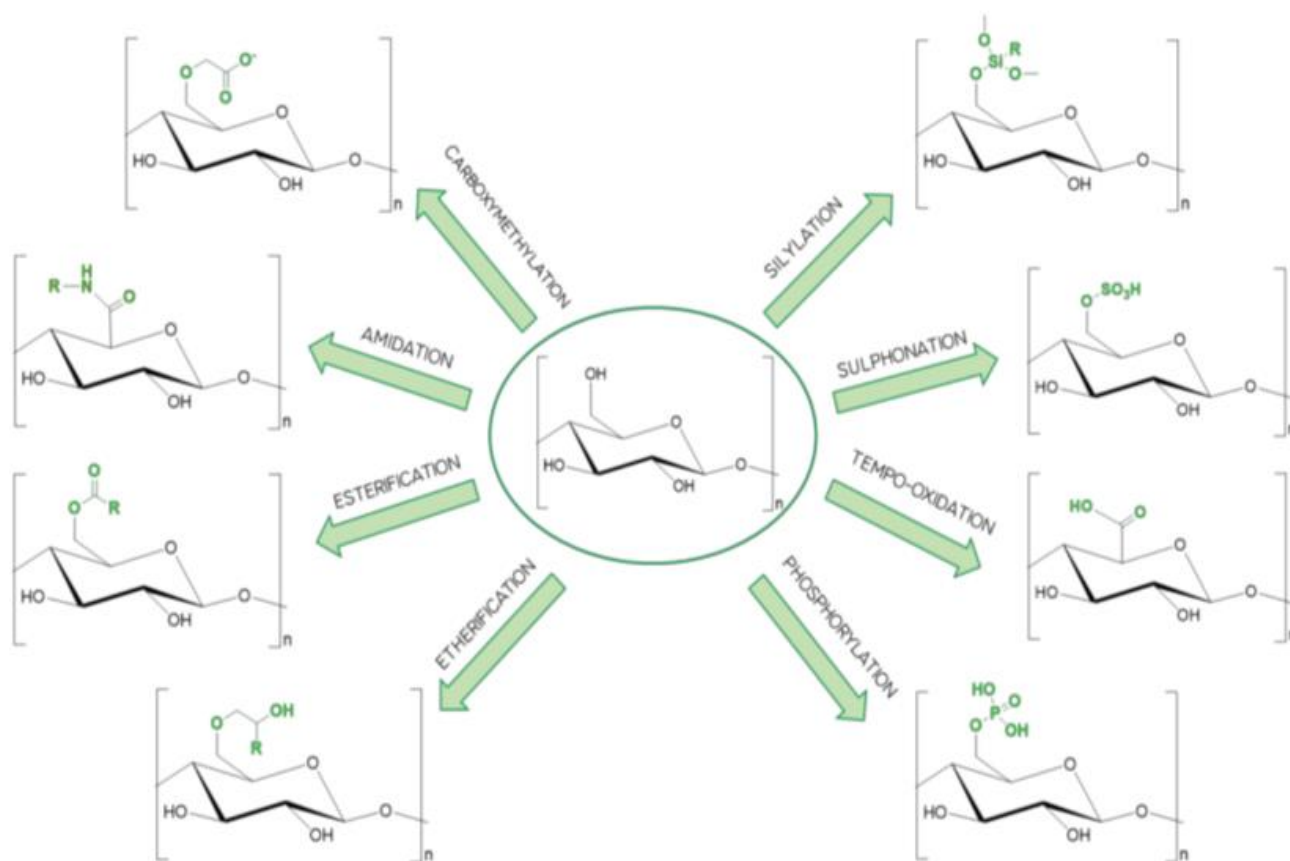


Figure 2. Different chemical functionalization of cellulose⁴³

Some examples of modified cellulose are phosphorylated nanocelluloses,³⁵ cellulose microsphere,³⁶ carboxy cellulose nanofibers (CNF),³⁷ microcrystalline cellulose-based porous material,³⁸ tricarboxylic cellulose,³⁹ carboxymethylated cellulose fiber (CMF),⁴⁰ organic-inorganic bionanocomposite,³⁴ poly(acryloyl hydrazide)-grafted cellulose nanocrystal particles (CNC-PAH),⁴¹ magnetic carboxymethyl chitosan nanoparticles,⁴² and microcrystalline cellulose. Modifications in the cellulose surface cause an increase in its reactivity in the chemical environment and facilitates the interaction with the other components of the mixture.

Amino groups functionalized adsorbents have an excellent ability to extract Cr (VI) from aqueous solution. Polyethyleneimine (PEI) has been considered as a source of amino groups to improve their chemical and physical properties due to PEI has strong binding affinity for various metals due to the existence of primary and secondary amine groups. Below are several synthetic strategies of cellulose–PEI composites. It is based on a compilation of information by Riva et al.⁴³ An alternative functionalization is the use of cross-linking with epichlorohydrin (EPI) and glutaraldehyde (GA) that allows a significant reduction in the reaction time and guarantees a more homogeneous heating of the mixture. Figure 3 show the formation of the cellulose–PEI composites using crosslinkers.

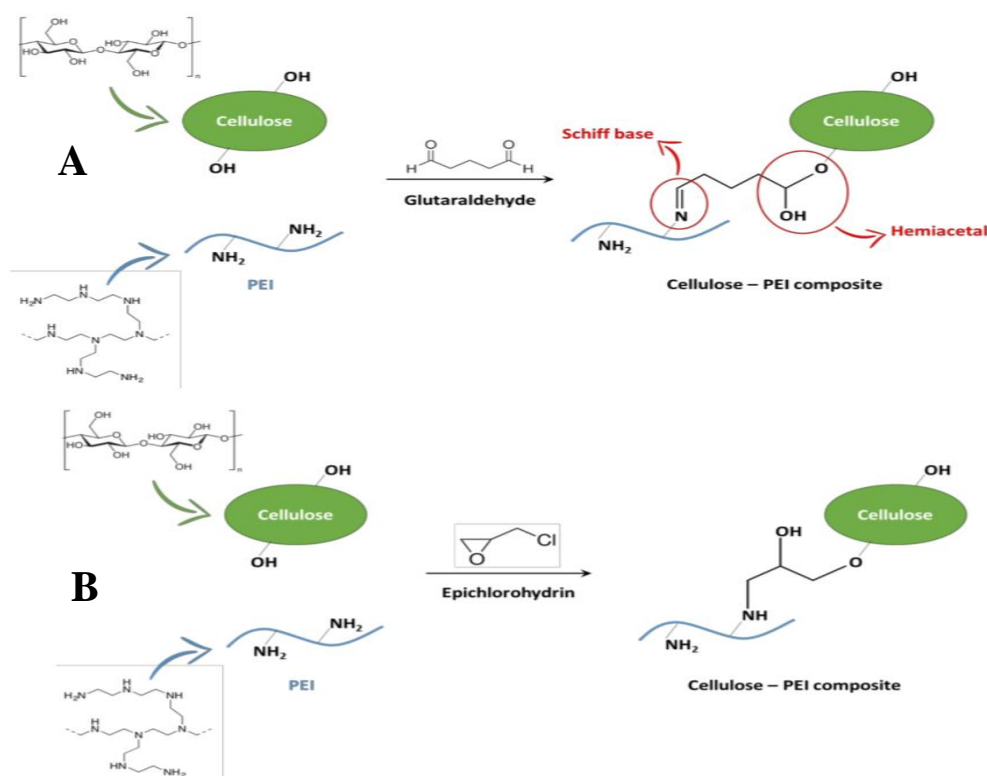


Figure 3. Cross-linking cellulose–PEI in the presence of (A) GA and (B) EPI⁴³

On the other hand, cellulose functionalization in the absence of crosslinking could also occur with the use of condensing agents such as EDC (1-ethyl-3-(3-dimethylaminopropyl)carbodiimide). EDC is capable of promoting the formation of amide bonds between amines from PEI and the carboxyl groups of cellulose oxidized with TEMPO. The advantage of this synthetic route lies in the possibility of operating at room temperature

Another pathway is to take advantage of the reactivity of active site-bearing silane derivatives, which can promote the formation of covalent bonds between cellulose hydroxyl and PEI amino groups (Figure 4). This grafting strategy allows the introduction of epoxy groups, which in turn can react with the amines present in PEI.⁴³ Cellulose functionalization should be considered essential to make it a powerful material, improving its structure for the elimination of Cr (VI).

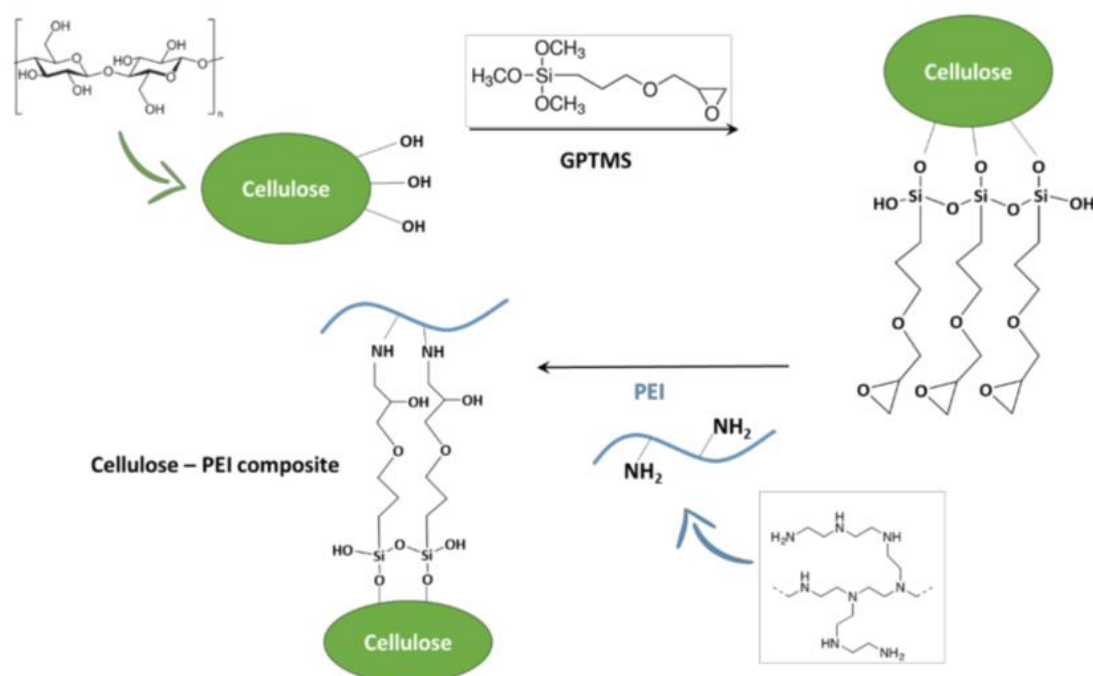


Figure 4. Preparation of cellulose-PEI xerogel scaffolds⁴³

4.2. Adsorption Kinetic Models

Adsorption kinetic models are used to evaluate the performance of the adsorbent and to examine the mechanisms of adsorption. The process of mass transfer during adsorption has been summarized in three steps as show in Figure 5.⁴⁴

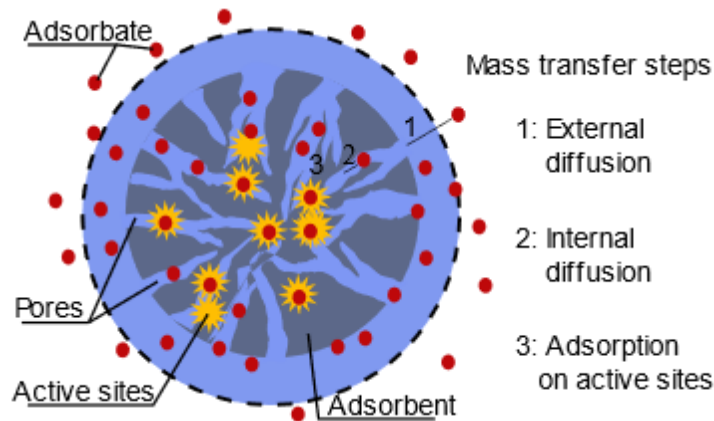


Figure 5. Schematic of the process of mass transfer during adsorption⁴⁴

- (1) External diffusion. The adsorbate diffuses through the thin liquid film around the adsorbent, driving by the difference in chemical potential between the adsorbate in the bulk solution and the adsorbate at the surface of the adsorbent.
- (2) Internal diffusion. The adsorbate diffuses in the pores of the adsorbent.
- (3) Adsorption of the adsorbate in the active sites of the adsorbent.

4.2.1. Adsorption Reaction Models

Different adsorption reaction models have been used to investigate the adsorption kinetic process. These models include: (1) empiric models (without specific physical meaning), (2) external diffusion models, which assume that the slowest step in the process is the diffusion of adsorbate from the bulk solution and through a boundary liquid film around the adsorbent, (3) internal diffusion models, which assume that the diffusion of adsorbate within adsorbent is the slowest step, (4) adsorption onto active sites models, which assume that the adsorption onto active site is the slowest step.⁴⁴

For far, the most applied models are the pseudo-first-order model (PFO), the pseudo-second-order model (PSO), the Ritchie equation, the Elovich model, and the phenomenological models of mass transfer to describe the kinetic process of adsorption.⁴⁴

Due to its simplicity, the linear regression method is the most widely used to fit data and obtain the parameters of adsorption models. However, the linearization process could introduce propagate errors to the independent/dependent variables, causing inaccuracy in the estimation of the parameters that is why it is advisable to use a nonlinear method to obtain consistent and accurate estimations for model parameters.⁴⁵

4.3. Experimental Characterization Techniques

4.3.1. Fourier Transform Infrared Spectroscopy (FTIR)

The Fourier Transform Infrared (FTIR) spectroscopy is a method for the quantitative analysis of complex mixtures. IR radiation is passed through a sample but some of the radiation is absorbed and some of it is transmitted. An IR spectrum represents the fingerprint of a sample, with absorption peaks that correspond to the frequencies of vibrations between the bonds of the atoms making up the material. Each material has a unique composition and different arrangement of atoms, and no two compounds produce the same IR spectrum. In addition, the size of a peak in the spectrum is an indicator of the amount of material present. Therefore, IR spectroscopy can result in a qualitative analysis of every kind of material, and with modern software algorithms, IR is an excellent tool for quantitative analysis.⁴⁶

4.3.2. X-Ray Diffraction (XRD)

X-ray Diffraction (XRD) is an analytical technique that is used mainly for the evaluation and quantification of the type and degree of crystallinity present in a material, providing information on its structure.⁴⁷ However, the powder XRD technique is the most widely used because of the ease with which it is performed and because it is a quick and accurate way to identify a mineral or mineral mixture.⁴⁸

4.3.3. Scanning Electron Microscopy (SEM)

The Scanning Electron Microscope (SEM) allows the characterization and morphology analysis of the microstructure of organic and inorganic materials from micrometer to nanometer scale.^{49,50} SEM irradiates with a fine focusing electron beam in the area to be micro analyze and the detector recover the signals.⁵¹ Some characteristics of SEM, high resolution, dynamic magnification range, microanalysis, and a greater depth of field that allows to obtaining images of rough sample surfaces.⁵²

Furthermore, energy dispersive spectroscopy (EDS) provides images of elemental distribution within a specific area correlated with the SEM images. EDS is used to identify existing elements and corresponding atomic proportions at the surface of functionalized cellulose.

4.3.4. Ultraviolet-Visible Spectroscopy (UV-Vis)

UV–Vis spectroscopy is a technique widely used for the characterization of materials that encompasses absorption spectroscopy and reflectance spectroscopy in the UV–Vis spectral region. Several UV-Vis configurations are available, including transmission, diffuse reflectance, and absorption. Also, with the help of the UV–Vis spectrum, the mechanism of complexation between templates, monomer, and cross-linker during polymerization can also be better understood. It has been observed that after complexation, an absorbance shift toward shorter wavelengths takes place.⁵³ Molecules containing p-electrons or non-bonding electrons (n-electrons) can absorb ultraviolet or visible light energy and be excited to higher anti-bonding molecular orbitals. Generally, UV–Vis spectroscopy is used to determine elemental concentrations quantitatively in a solution according to Beer–Lambert law:⁵⁴

$$A = \text{Log}_{10} \frac{I_0}{I} = \varepsilon c L \quad (1)$$

where:

A = measured absorbance

I_0 = intensity of the incident light

I = transmitted intensity

L = length through the sample

c = concentration of the absorbing specie

ε = molar absorptivity constant

4.3.5. X-Ray Photoelectron Spectroscopy (XPS)

X-ray photoelectron spectroscopy (XPS) is an indispensable technique in surface and materials science for the determination of chemical bonding by the analysis of oxidation states of each component. XPS is moreover referred to as a fingerprint technique, as each element has a unique set of associated core-level peaks that allow their identification.⁵⁵ XPS is the most widely used vacuum technique for chemically analyzing surfaces, can detect all the elements except hydrogen and helium, and through chemical shifts, it provides chemical state information about the elements.

CHAPTER III

5. Methodology

5.1. Materials, Reagents and Equipment

The rice husk was obtained of Quito-Sierra region of Ecuador. The reagents used during the development of this work are specified in Table 2, which was obtained in a particular way from advisors and was completed with the School of Chemical Sciences and Engineering resources. The equipment used was a hot plate magnetic stirrer, centrifuge (Centrifuge Centronic BLT), oven, coffee grinder (DAEWOO DCG-362), fume cupboard, which were used to complete the procedure.

Table 2. Reagents

Reagents	Description
Sodium Hydroxide	(NaOH) CAS:1310-73-2
Sodium Chlorite	(NaClO ₂) CAS:7758-19-2
Acetic Acid	(CH ₃ CO ₂ H) CAS:64-19-7
Distilled Water	(H ₂ O) CAS:7732-18-5
Glutaraldehyde	OHC(CH ₂) ₃ CHO CAS:111-30-8
Branched Polyethylenimine	H(NHCH ₂ CH ₂) _n NH ₂ CAS:25987-06-8
Ethanol	(C ₂ H ₅ OH) 96 % CAS:64-17-5
(3-Aminopropyl) triethoxysilane	H ₂ N(CH ₂) ₃ Si(OC ₂ H ₅) ₃ CAS:919-30-2
Chloroacetic Acid	ClCH ₂ COOH CAS:79-11-8

5.2. Extraction and Purification of Cellulose from Rice Husk

First of all, the RH dry was ground in a coffee grinder and sifted in different diameters and mesh (Figure 6B). To cellulose obtain was used two sizes: ground RH (Figure 6C) without sifted and RH powder. The delignification and bleached treatment of RH was according to Oliveira et al.⁵⁶ and the Johar et al.²⁸ with some modification. The changes were in proportions of reagents, methodology, and reaction time.

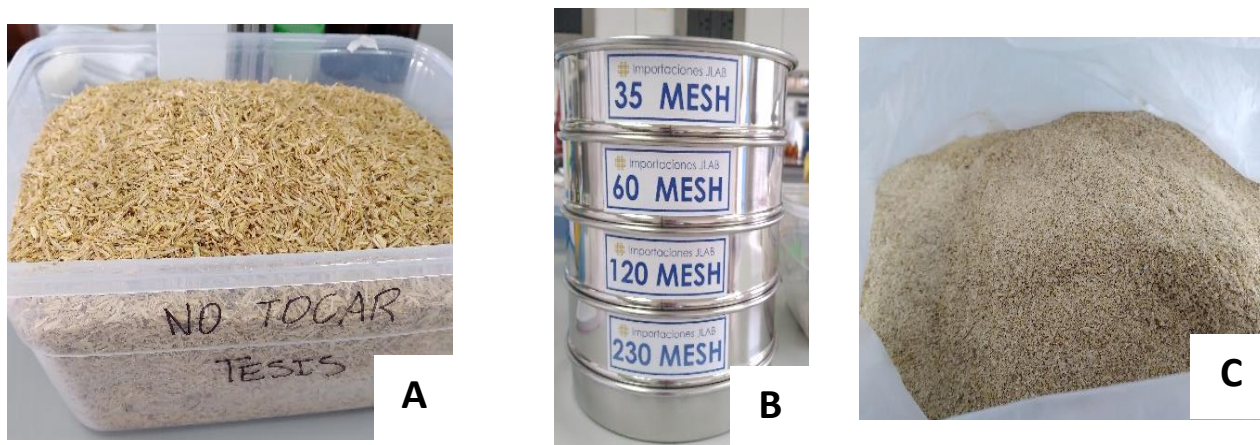


Figure 6. (A) Rice Husk, (B) Sieve, (C) Ground RH

5.2.1. Removal of Impurities: Alkaline Treatment

The RH was subjected to alkaline treatment to remove lignin and hemicellulose. 30 g of ground RH was treated with 600 mL NaOH (5 wt%). The mixture was transferred into an Erlenmeyer under magnetic stirring constantly at 80 °C for 4 h. In the end, the product was neutralized until pH of 7 and centrifuge three runs at 2500 rpm for 10 min with distilled water and dried at 40 °C in the oven.

5.2.2. Purification of Crude Cellulose: Cellulose Bleaching

The bleaching process was completed by removing the lignin from the RH obtained in the alkaline treatment. In an Erlenmeyer added the previously treated RH, 18 g sodium chlorite (NaClO_2), 12 mL glacial acetic acid (CH_3COOH), and 975 mL distilled water at 70 °C for 3 h and stirring continually. Each hour added the same volume of CH_3COOH and NaClO_2 to the mixture. The mixture was cold, and centrifuge three runs at 2500 rpm for 10 min with distilled water and dried at 40 °C in the oven.

5.3. Preparation of Bioadsorbents

For the modification and functionalization of the cellulose surface, three different processes were used. Two processes were based on the previous works by Chen et al.,⁵⁷ Neves et al.,⁵⁸ Boufi et al.,⁵⁹ and Shui et al.⁶⁰ with some modifications in concentrations of reagents, methodology, time and reagents. The last process is a proposal of two-step. In the first step, cellulose is modified with APTES and in the second step, cellulose modified is functionalized with bPEI. This process has the aim to increase the active sites in the structure to improve the adsorption process.

5.3.1. Synthesis Functionalized Cellulose with bPEI (K-FCPG)

Functionalized cellulose with bPEI and GA as a crosslinking agent. This functionalization process was repeated for each modified cellulose with the name "FCPG". Procedure reported by Chen et al.⁵⁷ was followed with some modifications. Briefly, 1 g of cellulose was dispersed in 100 mL of distilled water under magnetic stirring for 16 h at room temperature. This process was to increase the superficial area of cellulose for prepare of functionalization. At the end of the time, 1 g bPEI was added into the suspension in stirring continuously and heated to 45 °C to add 1.5 g of GA in vigorous stirring for 3 h. Finally, the product was centrifuged for three runs at 2500 rpm for 10 min with distilled water. Then, the residue was dried at 40 °C in the oven Figure 7 shows the schematic way of the

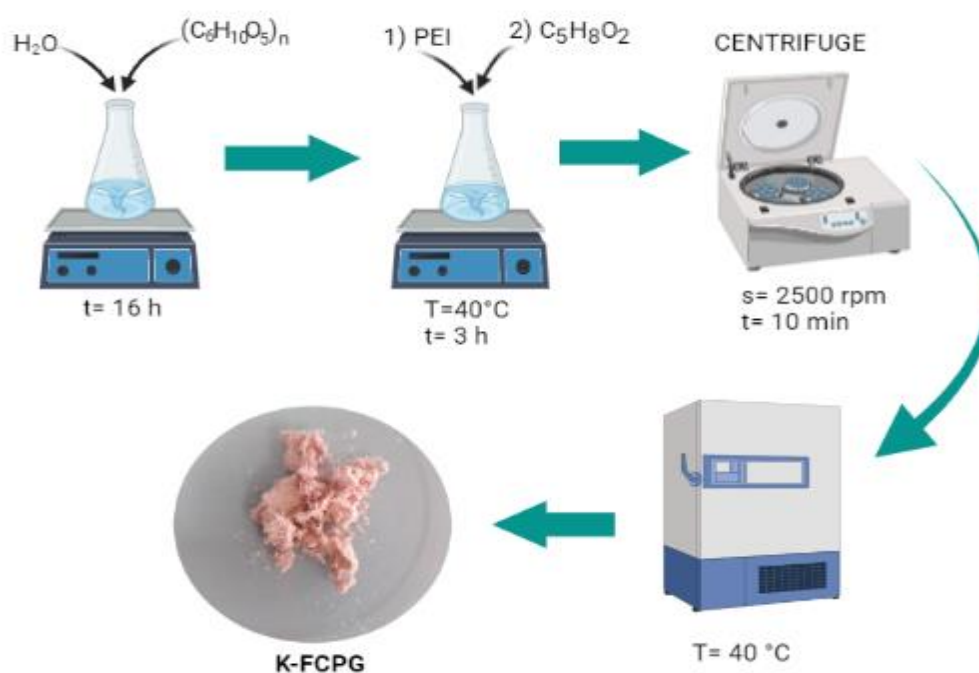


Figure 7. Schematic illustration of the synthesis of K-FCPG

5.3.2. Synthesis of APTES Modified Cellulose (K-APTES)

The modified cellulose with APTES was following the procedure according to Neves et al.⁵⁸ and Boufi et al.⁵⁹ with some changes. The first step is the hydrolysis of APTES was done with 5 mL APTES and 100 mL distilled water. The solution was acidified with CH_3COOH to a pH of 4 under magnetic stirred for 30 min. Then, add 1 g cellulose to the mixture and dispersed in an ultrasonic bath for 10 min at 25 °C. After, the mixture was stirred for 2 h at room temperature. The cellulose modified was centrifuge two runs at 2500 rpm for 10 min with distilled water to dispersed and in the oven at 105 °C for 15 min to perform the reaction. After 15 min at oven, the modified cellulose was centrifuged three times, two washed with $\text{C}_2\text{H}_5\text{OH}$ (96 %) and one time with distilled water to remove unreacted APTES. The solid residue was dried at 40 °C in the oven and stored. Figure 8.a show schematic illustration of K-APTES obtention.

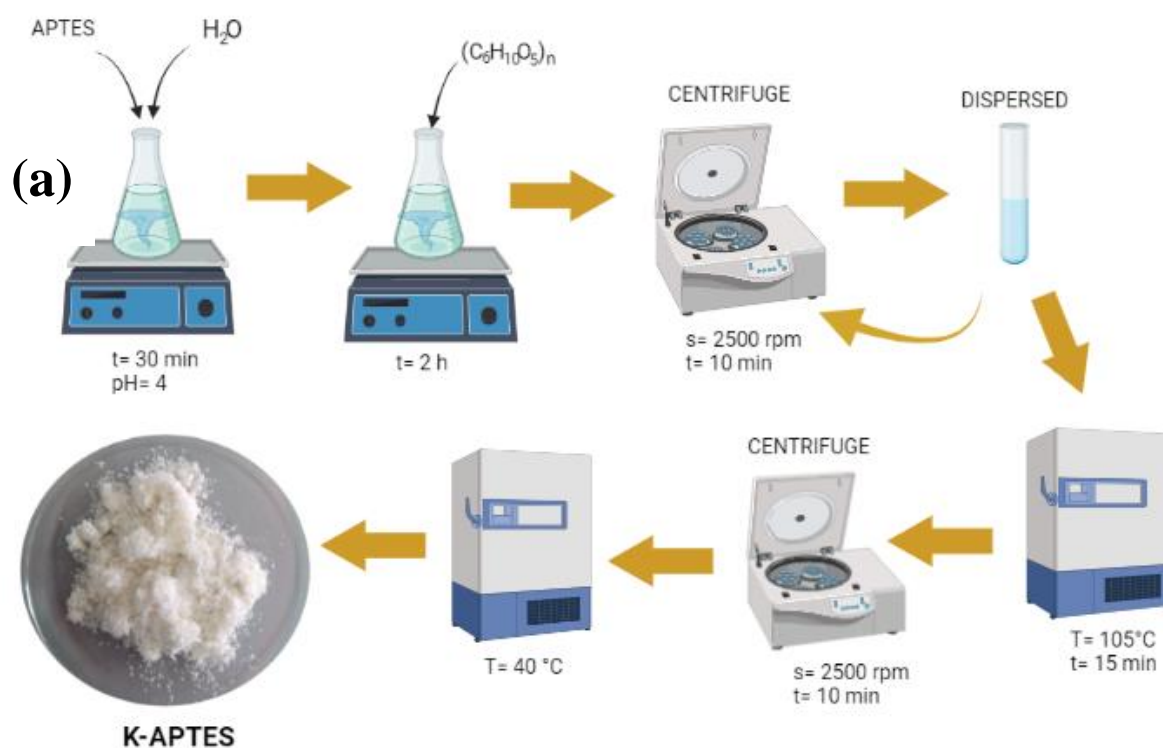


Figure 8. (A) Schematic illustration of the synthesis of K-APTES

5.3.3. Synthesis of Carboxymethyl Cellulose (K-CMC) and Functionalized with bPEI (K-CCFCPG)

The synthesis of the K-CMC procedure can be described in three steps alkalization, etherification, and neutralization. The procedure reported by Shui et al.⁶⁰ was followed with some modifications. 1 g bleached cellulose was treated with 1g NaOH (50 wt%) solution and 10 mL distilled water for alkalization use. Then, the beaker was covered and left in the water bath at 35 °C for 1h under slow stirring. After that, prepare a premix of 1 g NaOH (50 wt%) solution with 1.6 g chloroacetic acid. The premix was diluted in 35 mL ethanol (95 vol%) and added to the beaker. The solution was heated at 75 °C for 1.5 h to 2500 rpm for cellulose etherification. In the end, the mixture was cooled and neutralizing with hydrochloric acid, centrifugate three times with ethanol (95 vol%). Finally, the solid residue was dried at 40 °C in the oven. After synthesis, K-CMC was functionalized through the FCPG process (Figure 9) and was stored with the K-CCFCPG name.

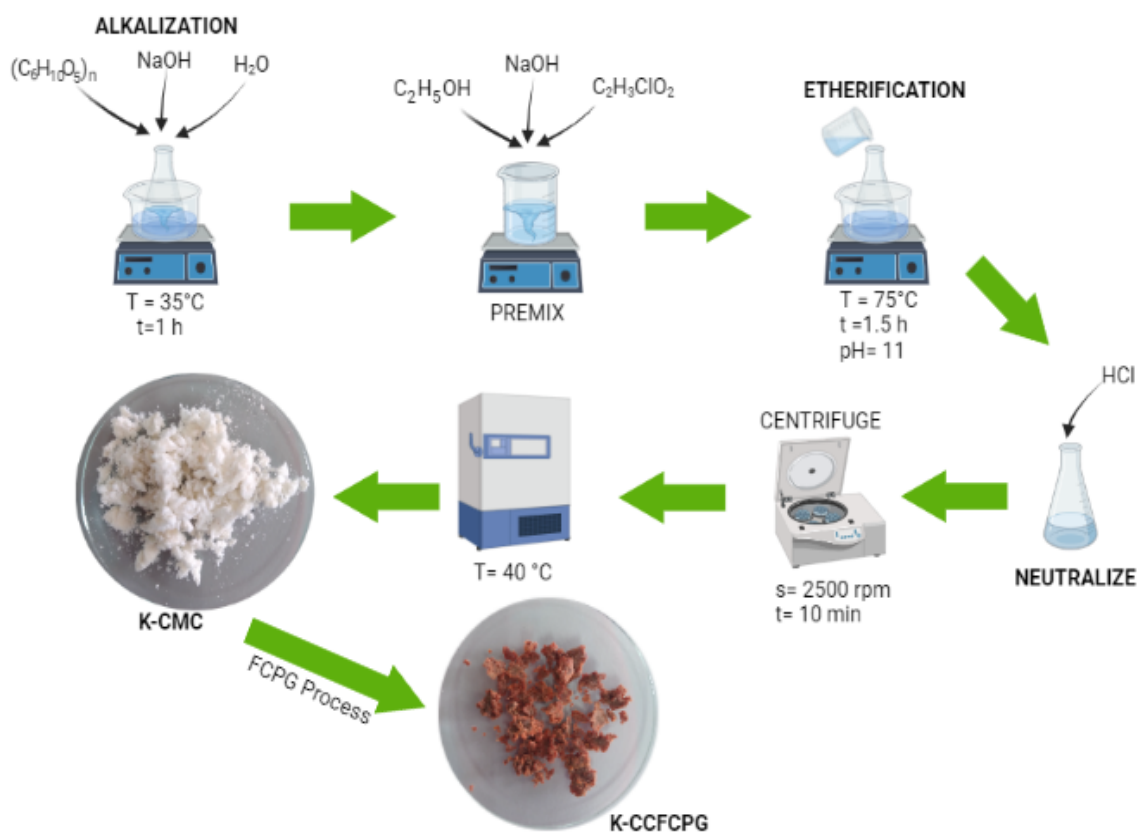


Figure 9. Schematic illustration of the synthesis of K-CMC and K-CCFCPG

5.3.4. Synthesis Functionalized Cellulose with bPEI (K-AFCPG)

K-AFCPG is a new material that was synthesized in two steps. The first step was the modification of K-APTES (Figure 8.a), and the second step was functionalized with bPEI and GA. Figure 10.b show the synthesis for the second part. Following the FCPG procedure. 1 g of K-APTES was dispersed in 100 mL of distilled water under magnetic stirring. Then bPEI was added and heat at 40 °C to then Glu added. After 3 h, the product centrifuged for three runs with distilled water. The solid was dried at 40 °C and stored.

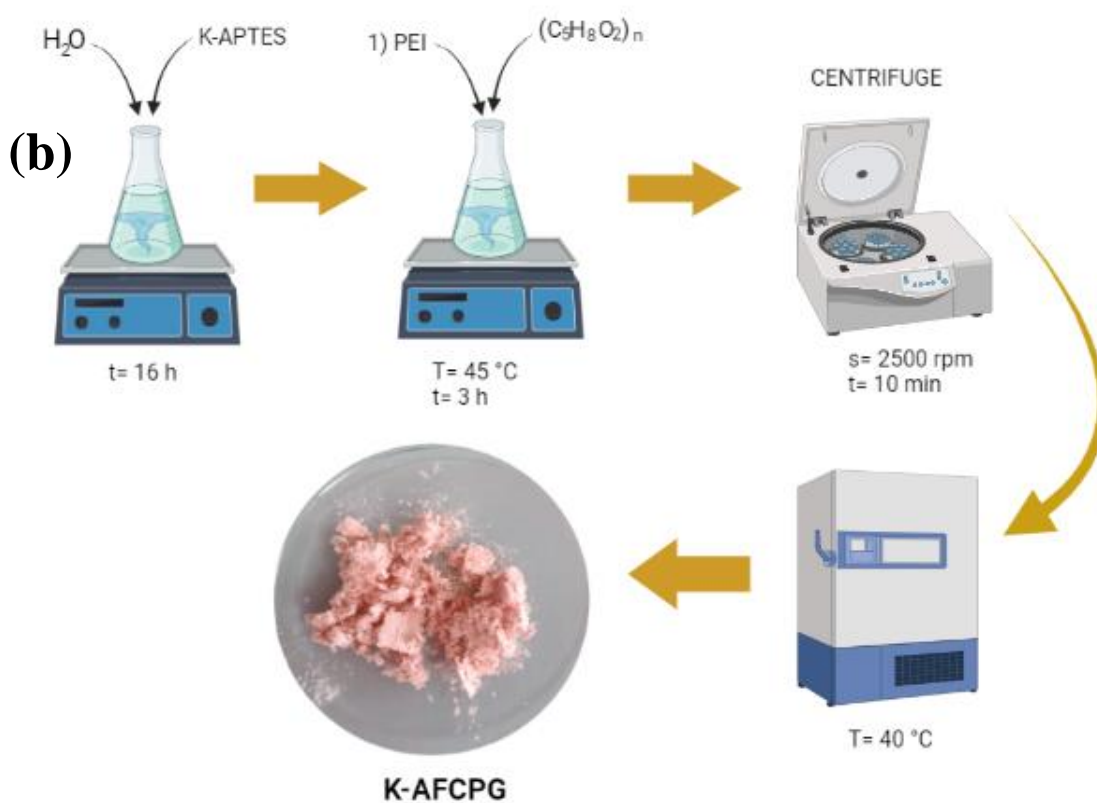


Figure 10. Schematic illustration of the synthesis of K-AFCPG

5.4. Design of Adsorption Experiments

5.4.1. Kinetic Batch Studies on Cr (VI) Adsorption

A series of batch experiments were programmed, where 100 ppm of Cr (VI) solution was added 5 mL on volumetric flasks that containing 5, 10, 15, and 20 mg of K-FCPG. The same process was used to K-AFCPG, and K-CCFCPG. Table 3 show the specific weight used for the experiment in each case. All experiments were performed under ambient conditions and samples were gently shaken by hand during the measurement time, to establish adsorption equilibrium. Then, 3 mL of the liquid phase of each solution obtained were added to a quartz cell, light absorbance of the samples was measured at 352 nm using a spectrophotometer, and the results were used to calculate the amount of adsorption perused sorbents, at equilibrium (q_e).

Table 3. Specific weight used for the batch experiment

Batch Experiments				
Materials	5 mg	10 mg	15 mg	20 mg
K-AFCPG	5.1 mg	10.0 mg	15.5 mg	20.5 mg
K-FCPG	5.7 mg	10.3 mg	15.2 mg	20.7 mg
K-CCFCPG	-	-	15.3 mg	-

5.4.2. Data Analysis of Adsorption Kinetics

Nine different kinetic models⁴⁴ were considered to describe the data. In Table 4, the differential and integrated form of the equations for each model is showed.

Table 4. Kinetics Models

Models	Differential equation	Integrated form
Pseudo first order PFO	$\frac{dq_t}{dt} = k_1(q_e - q_t)$	$q_t = q_e(1 - e^{-k_1 t})$
Pseudo second order PSO	$\frac{dq_t}{dt} = k_2(q_e - q_t)^2$	$q_t = \frac{q_e^2 k_2 t}{1 + q_e k_2 t}$
Mix order	$\frac{dq_t}{dt} = k_1(q_e - q_t) + k_2(q_e - q_t)^2$	-
Elovich	$\frac{dq_t}{dt} = ae^{bq_t}$	$q_t = \frac{1}{b} \log(1 + abt)$
Boyd's external diffusion	$\frac{dq_t}{dt} = R(q_\infty - q_t)$	$q_t = q_\infty(1 - e^{-Rt})$
Frusawa and Smith	-	$\frac{C_t}{C_0} = \frac{1}{1 + m_s K} + \frac{m_s K}{1 + m_s K} e^{-\frac{1+m_s K}{m_s K} k_{F\&S} t}$
Boyd's intraparticle diffusion	-	$Bt = -\ln \frac{\pi^2}{6} (1 - F)$
Weber and Morris	-	$q_t = k_{W\&M} t^{1/2}$
Langmuir	$\frac{dq_t}{dt} = k_a \left(C_0 - \frac{mq_t}{V} \right) (q_{max} - q_t) - \frac{k_a}{K_L} q_t$	-

The abbreviations of equations are:

a Initial adsorption rate constant of the Elovich model (mg·g⁻¹)

A Constant of the Boyd's equation

b Desorption rate constant of the Elovich model (g·mg⁻¹)

B Boyd's coefficient (min·h⁻¹)

*C*₀ Initial adsorbate concentration (mg·L⁻¹)

C_e Equilibrium adsorbate concentration ($\text{mg}\cdot\text{L}^{-1}$)

C_t Adsorbate concentration at time t ($\text{mg}\cdot\text{L}^{-1}$)

k_1 Pseudo-first-order rate constant (min^{-1})

K_2 Pseudo-second-order rate constant (min^{-1})

K_a Adsorption rate constant ($\text{L}\cdot\text{mg}^{-1}\cdot\text{min}^{-1}$)

$k_{F\&S}$ Mass transfer coefficient between the bulk liquid and the surface of the adsorbent ($\text{cm}\cdot\text{min}^{-1}$)

K_L Langmuir constant ($\text{L}\cdot\text{mg}^{-1}$)

$K_{W\&M}$ Intraparticle diffusion coefficient ($\text{mg}\cdot\text{g}\cdot\text{min}^{-1/2}$)

m_s Mass of adsorbent per unit volume of solution ($\text{g}\cdot\text{L}^{-1}$)

q_∞ Equilibrium adsorption capacity at infinite time ($\text{mg}\cdot\text{g}^{-1}$)

q_{cal} Calculated adsorption capacity ($\text{mg}\cdot\text{L}^{-1}$)

q_e Adsorption capacity at equilibrium ($\text{mg}\cdot\text{L}^{-1}$)

q_{et} Equilibrium adsorption capacity in the pores of the adsorbent ($\text{mg}\cdot\text{g}^{-1}$)

q_{exp} Experimental adsorption capacity ($\text{mg}\cdot\text{L}^{-1}$)

q_m Maximum adsorption capacity ($\text{mg}\cdot\text{g}^{-1}$)

q_{max} Langmuir constant ($\text{mg}\cdot\text{g}^{-1}$)

q_t Adsorbed amount of the adsorbate at time t ($\text{mg}\cdot\text{L}^{-1}$)

t Adsorption time (min)

V Solution volume (L)

5.5. Characterization Techniques

5.5.1. Fourier Transform Infrared Spectroscopy- Attenuated Total Reflectance (FTIR-ATR)

Fourier Transform Infrared Spectroscopy-Attenuated Total Reflectance (FTIR-ATR) was used to characterize the functional groups of K-FCPG K-APTES K-CCFCPG, and K-AFCPG to check if the cellulose has been modified. Also, this technique was also conducted to verify if K-FCPG and K-AFCPG were saturated with Cr (VI) after adsorption. The samples were studied by FT-IR using a Cary 630 with a 1-Bounce Diamond ATR accessory. The spectra were obtained in the range of 4000–400 cm^{-1} , with a spectra resolution of 4 cm^{-1} and 128 scans. Thermo Scientific OMNIC 9 software was used to process data.

5.5.2. X-Ray Diffraction (XRD)

The X-Ray Diffraction (XRD) patterns were collected by using a Mini-flex-600 from Rigaku, with a D/tex Ultra2. The X-Ray generator, Ni-filtered Cu $K\alpha$ radiation ($\lambda=0.15418$ nm) at 40 kV and 15 mA. The powder samples were placed at $2\theta = 5^\circ - 90^\circ$ with a step width of 0.01° . To determine the crystallinity index (CrI) of cellulose type I used the Segal method^{61,62} described in equation 2. The empirical method proposed by Segal was chosen due to it is commonly used in cellulose⁶².

$$CrI\% = \frac{I_{002} - I_{am}}{I_{002}} \times 100 \quad 2$$

where I_{002} corresponds to the height of the peak corresponding to the (0 0 2) plane, and I_{am} is the lowest height of the sample.

5.5.3. Scanning Electron Microscopy/Energy Dispersive X-Ray Spectrometer (SEM/EDS)

A Scanning electron microscopy/energy dispersive X-ray spectrometer (SEM/EDS) Phenom ProX desktop was used to perform the elemental microanalysis of the K-FCPG K-AFCPG K-CCFCPG. SEM-EDS working with an acceleration voltage of 10 kV, with a backscatter electron detector, which gives images with the contrast between the elements with different atomic numbers.

5.5.4. Ultraviolet- Visible Spectroscopy (UV-Vis)

The spectrophotometer used was a UV/Vis/NIR LAMBDA 1050 from Perkin Elmer, double beam, double monochromator, with holographic grating with 1440 lines/mm, UV/Vis blazed at 240 nm, Littrow mounting. Photomultiplier R6872 for high energy in the entire UV/Vis wavelength range. The light sources used are tungsten-halogen and Deuterium. The Operating Range is 175-3300 nm, ≤ 0.05 nm. The system is controlled by WinLab software.

5.5.5. X-Ray Photoelectron Spectroscopy (XPS)

X-ray photoelectron spectroscopy (XPS) analysis was performed on K-FCPG, and K-AFCPG saturated with Cr (VI). The samples were placed onto a polymeric-based adhesive tape that was held in a metallic mesh. X-ray photoelectron spectroscopy uses a PHI 5000 Probe III Scanning XPS Microprobe from Ulvac phi, inc. The spectra were calibrated using the signal of carbon at 284.8 eV. Also, for high-resolution deconvolution was using Tougaard background subtractions and Voigtian and Gaussian functions. The software used for this purpose was Fityk.⁶³

CHAPTER IV

6. Results and Discussion

6.1. Extraction and Characterization of Cellulose from Rice Husk

The rice husk was crushed and then sieved through different mesh sizes. Two sizes of husk were used for the extraction of cellulose. The first size is crushed rice husk that would be the largest and the second size is rice husk powder >230 or >63 μm . Both rice husk sizes were subjected to alkaline treatment (Figure 11A) and bleaching (Figure 11B). After the chemical treatments, rice husk color changed from brown to white due to the removal of non-cellulosic materials such as lignin, hemicelluloses, pectin, and wax upon chemical treatment of the rice husks. Regarding the yield of the process for obtaining cellulose, it was 12.5 g of cellulose / 30 g of RH equivalent to 41.7%. The yield obtained is rich compared to the process of Oliveira et al.⁶⁴ that was 19.8 g cellulose/100 g of RH equivalent to 19.8% . Figure 11C shows the final cellulose from crushed RH, and Figure 11D shows the final cellulose from RH powder.

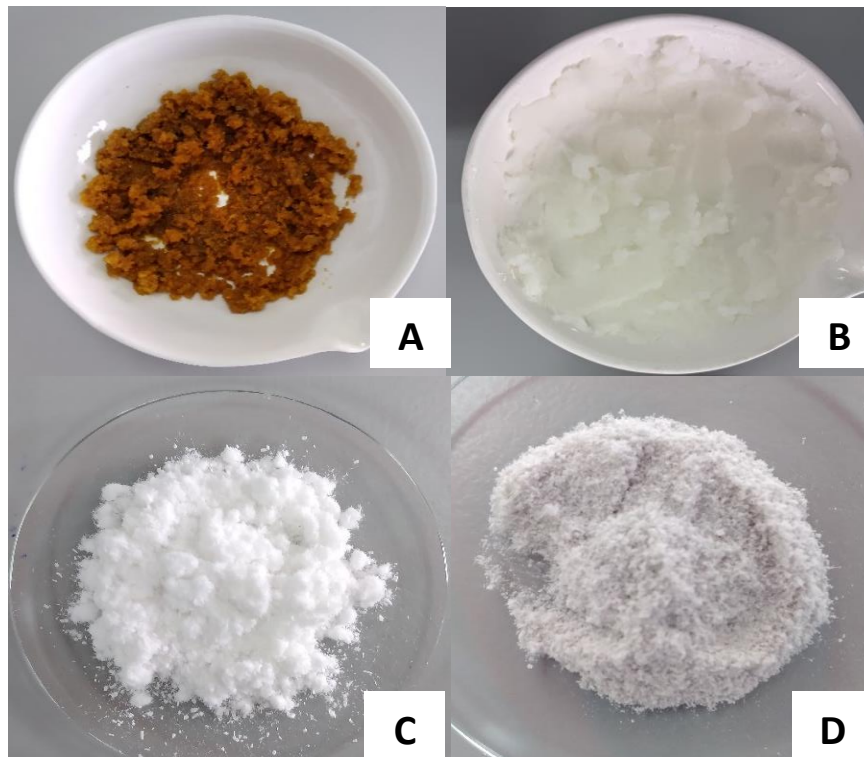


Figure 11. (A) RH after alkaline treatment, (B) RH after bleaching process, (C) Bleached Cellulose: crushed RH, and (D) Bleached Cellulose: RH powder

6.1.1. FTIR–ATR Analysis

The FTIR–ATR spectra of the both cellulose sizes were analyzed but there were no differences. Therefore, the characterization and surface modifications were made over from crushed RH. FTIR–ATR spectrum of cellulose in the Figure 12 shows a broadband in rang of 3100 at 3550 cm^{-1} was attributed to -OH stretching vibration, and a 2884 and 1424 cm^{-1} referred to C-H stretching vibrations.^{65,66} The band at 1313 cm^{-1} related to the bending vibrations of hydroxyl groups.⁶⁷ The peaks at 1101, 1051, and 1025 cm^{-1} are involved a strong C-O stretching of COH/C-O-C pyranose ring skeletal vibration,^{68,69} and another peak at 896 cm^{-1} attributed to β -glycosidic linkages between the sugar units in cellulose.^{59,70} Moreover, at 1422 cm^{-1} reflect the crystalline band of cellulose, and 896 cm^{-1} referred to the amorphous region.¹⁸ The IR spectrum of the cellulose obtained showed no lignin and hemicellulose after the mentioned treatments. This can be evidenced by the absence of the peaks at 1254, 1508, 1604 cm^{-1} correspond to the aromatic skeletal vibrations of lignin.^{18,71}

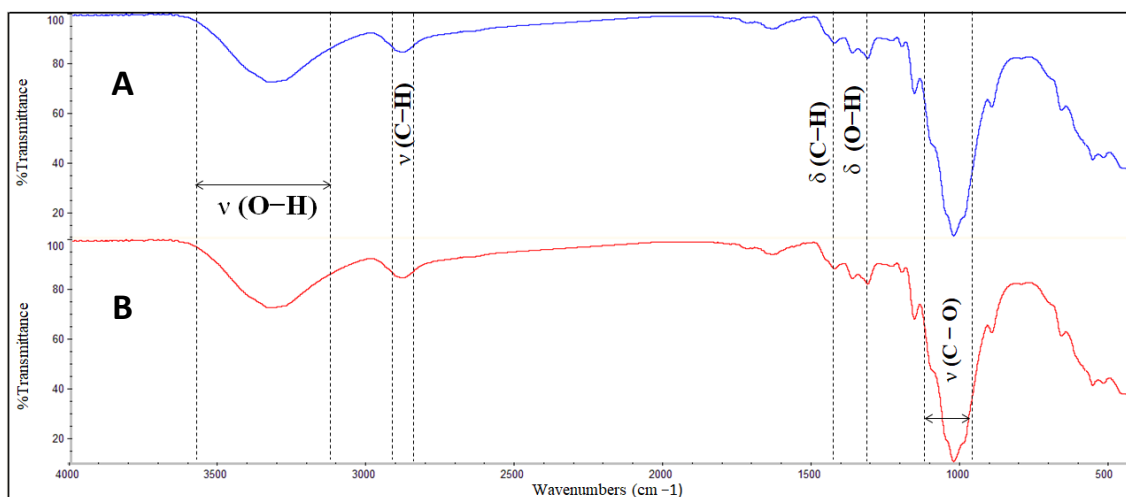


Figure 12. FTIR–ATR spectrum of (A) cellulose of crushed RH, and (B) cellulose of RH powder

6.1.2. XRD Analysis

XRD was used to evaluate the crystallinity of the cellulose obtained after chemical treatment of RH. After the alkaline treatment, the cellulose increase the rigidity since the impurities present were removed.²⁸ Figure 13 shows the cellulose XRD pattern, it has three well-defined crystalline peaks around $2\theta = 15.9^\circ$, 22.1° , and 34.8° ⁶⁴ are assigned to (1 0 1), (0 0 2), and (0 0 4) crystallographic plane. The crystallinity of cellulose may be due to hydrogen bonding interactions and Van der Waals forces between molecules.⁷² Also, the crystallinity index (CrI) of cellulose calculate by Segal method was 72.5% high to the cellulose nanocrystals obtained by Johar et al.²⁸ In other words, the cellulose obtained can be considered to be crystalline.

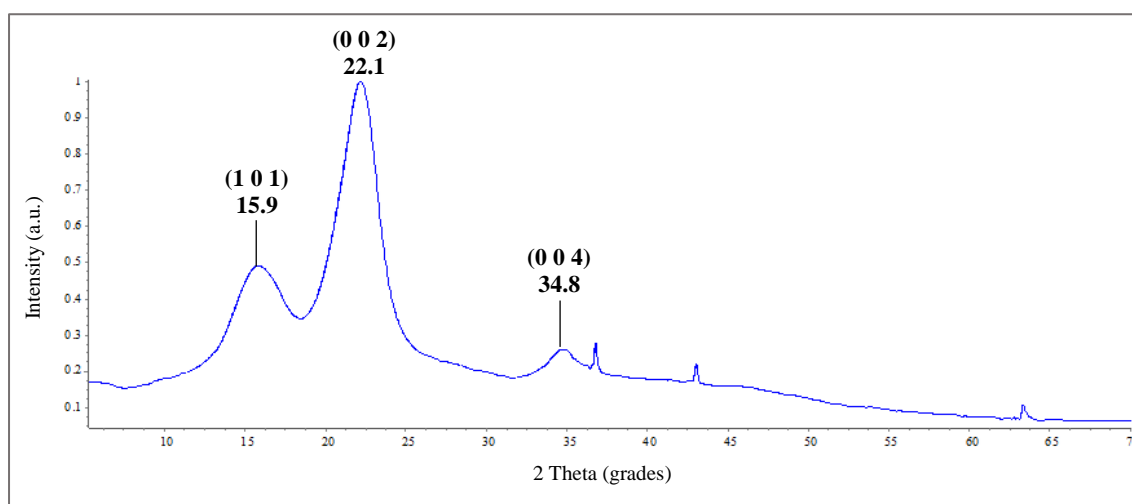
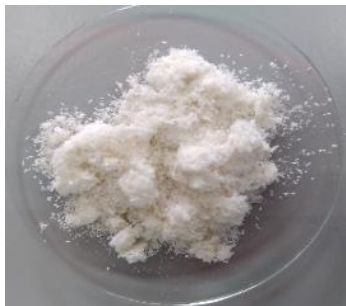


Figure 13. X-ray Diffraction pattern of cellulose

6.2. Synthesis Results

Four processes of modification of the cellulose surface were carried out. Table 5 shows a summary of observations, visible changes, and yield of the synthesized bioadsorbents.

Table 5. Synthesis of bioadsorbents results

Bioadsorbent	Observations and yield	Material
K-FCPG	<p>Cellulose was functionalized with bPEI and GA as a crosslinking agent to obtain K-FCPG. In general, the principal and more evident is the color change. It was the main signal to indicate that the initial cellulose had changed. In this case, K-FCPG shows a solid pink color. The functionalization cellulose process is efficient and can be evidence by the reaction yield due to the increase in the mass of bioadsorbent.</p>	
K-APTES	<p>This process is the first part of the K-AFCPG synthesis proposal. K-APTES is the result of the modified cellulose with APTES. During the process, the color of cellulose changes from white to pale yellow. The final color of K-APTES has been considered as an indicator that the cellulose structure has changed. The reaction yield was 0.87 g of K-APTES /1.003 g of cellulose that represented 87.0%. In other words, there is a loss of material that different aspects can cause. One of them could be that when the solid is recovered so you must be very careful.</p>	

**K-CMC and
K-CCFCPG**

The K-CMC is the first part of the K-CCFCPG synthesis. During the alkalization and esterification process, cellulose is modified to CMC to later be functionalized with bPEI. bPEI was used to increase the number of active sites on the cellulose surface. In the functionalization process, it was observed that K-CMC went from being a light white material to a rigid reddish material. The yield of the synthesis was 0.88 g of K-CCFCPG /1.007 g of cellulose that represented 87.4 %. This means that material was lost in the synthesis process.

**K-AFCPG**

The K-AFCPG is the proposal of a new material that has been previously modified with APTES to be later functionalized with PEI to increase active sites on the cellulose surface. This process took about 2 days, and it is simple and easy to replicate. In addition, during the functionalization process, the color of the K-APTES changes over time to solid pink color. Its mean, the synthesis process is efficient and confirms that new functional groups have been added to the cellulose surface.



* The yield of K-FCPG and K-AFCPG could not determine due to the material still having moisture.

As shown in Table 5, four types of cellulose have been functionalized and show different characteristics. In the case of K-CCFCPG and K-APTES, the reaction yield has been high than 80%, so the methodology used was efficient. But is necessary to be careful when recovering the material. K-FCPG and K-AFCPG were functionalized with bPEI and change color by a solid pink color. Also, the yield does not possibly determine due to the material has wet. In addition, similarity has been seen between the materials that are functionalized with PEI principally in the color. In other words, the PEI gives color to the adsorbent. However, the shade of pink varies depending on the type of cellulose to be functionalized.

Furthermore, another bioadsorbent was synthesized using cellulose obtained from RH powder (K-FCPG2). The cellulose was functionalized following the same procedure for the synthesis of K-FCPG. This new bioadsorbent had a pink color same as K-FCPG (Figure 14). In the same way as K-FCPG and K-AFCPG the yield could not be calculated to be able to compare it.



Figure 14. K-FCPG2 bioadsorbent

On the other hand, two crosslinker addition methods have been tested in blanched cellulose and K-APTES. In the first method, the GA was added drop by drop to the cellulose solution, and the other way was to add the GA abruptly. A homogeneous mixture was observed when the GA was added drop by drop. However, in the second case, lumps were formed in the solution. The final materials have color differences. As a result of the first method, K-PGG and K-AGG of pastel pink color were obtained, while

K-FCPG and K-AFCPG of pink color were obtained with the second method. The difference in colors can be seen in Figure 15.

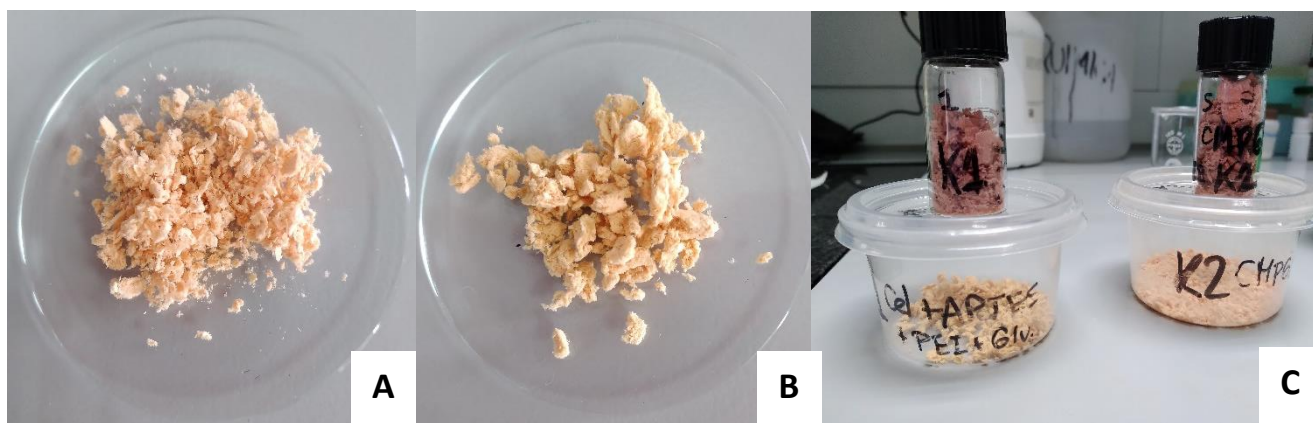


Figure 15. (A) K-PGG bioadsorbent, (B) K-AGG bioadsorbent, and (C) Comparison between two methods of add GA

6.3. FTIR-ATR Analysis

The FTIR–ATR technique was used to identify the different functional groups that have been introduced on the surface K-FCPG, K-APTES, K-CCFCPG, and K-AFCPG synthesized biomaterials. In addition to evaluating the variation of the structure after the functionalization processes.

6.3.1. K-FCPG Bioadsorbent

Compared to the FTIR–ATR spectra of cellulose (Figure 16A) with K-FCPG bioadsorbent, Figure 16 shows a broad band ranging from 3500 to 3100 cm^{-1} , which has been assigned to the overlapped stretching vibration of O–H of hydroxyl groups of cellulose and N–H amino groups of bPEI.⁷³ Appears at 2907 cm^{-1} , and 2852 cm^{-1} referred to C–H stretching, and the peak at 1653 cm^{-1} is of C=N stretching, indicating that crosslinking has taken place between primary amine groups of bPEI and GA, forming Schiff's base.⁷⁴ Another absorption peak at 1562 cm^{-1} associated with the N–H bending vibration was attributed to the terminal amine of bPEI.⁷⁵ Moreover, the new band that appeared at 1437 cm^{-1} represented the symmetric bending of NH_3^+ vibrations.⁷⁶ At 1050 – 1150 cm^{-1} appears a higher peak intensity which is ascribed to C–O stretching proving that GA is linked to cellulose chains.⁷⁷ These results confirmed that amino groups were introduced onto the cellulose surface, and the K–FCPG was successfully functionalized.

In addition, the FTIR–ATR spectra of K-FCPG and K-FCPG2 were compared, which were synthesized in the same way but with different cellulose sizes. K-FCPG2 shows two absorption bands more pronounced at 2907 and 2852 cm^{-1} corresponding to symmetric CH_2 and asymmetric CH_2 of the bPEI chains appeared.⁷⁸ In general K-FCPG (Figure 16A) and K-FCPG2 (Figure 16B) show the same signals to functional groups it is mean that in this case the particle size does not show differences in the structure.

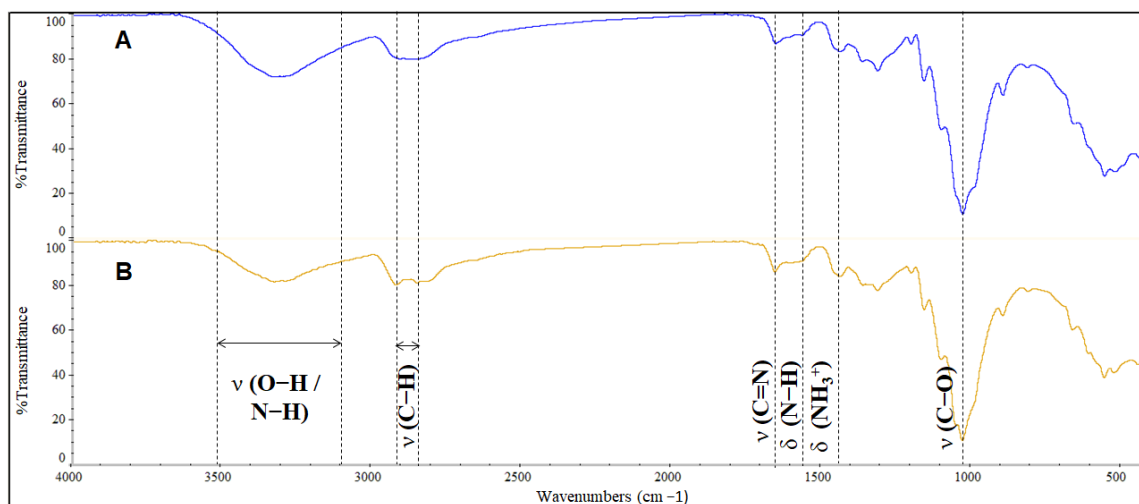


Figure 16. FTIR–ATR spectrum of (A) K-FCPG bioadsorbent and (B) K-FCPG2 bioadsorbent

6.3.2. K-APTES Bioadsorbent

Another spectrum analyzed is of K-APTES bioadsorbent. Figure 17 shows IR-bands of –OH of the hydroxyl groups and show new broadband slightly shifts to 1608 cm^{-1} can be attributed to the N–H bending vibration of primary amine, indicating that the functional groups such as amine and alcohol groups were introduced onto the surface cellulose.⁶⁹ Additionally, the bands corresponding to the Si–O–Si at 1101 cm^{-1} and Si–O–Cellulose bridges at 1159 cm^{-1} , were overlapped with the C–O vibration bands at 1026 cm^{-1} of cellulose.⁵⁸ The amino group of modified cellulose with APTES has higher reactivity than the hydroxyl group. In the FTIR spectrum, the vibration of the ether group between cellulose and APTES cannot be identified because it overlaps in the 1040 cm^{-1} region. However, the vibration of N–H of the amino group appears, confirming the modification resulted in K-APTES bioadsorbent with primary amino groups of APTES.

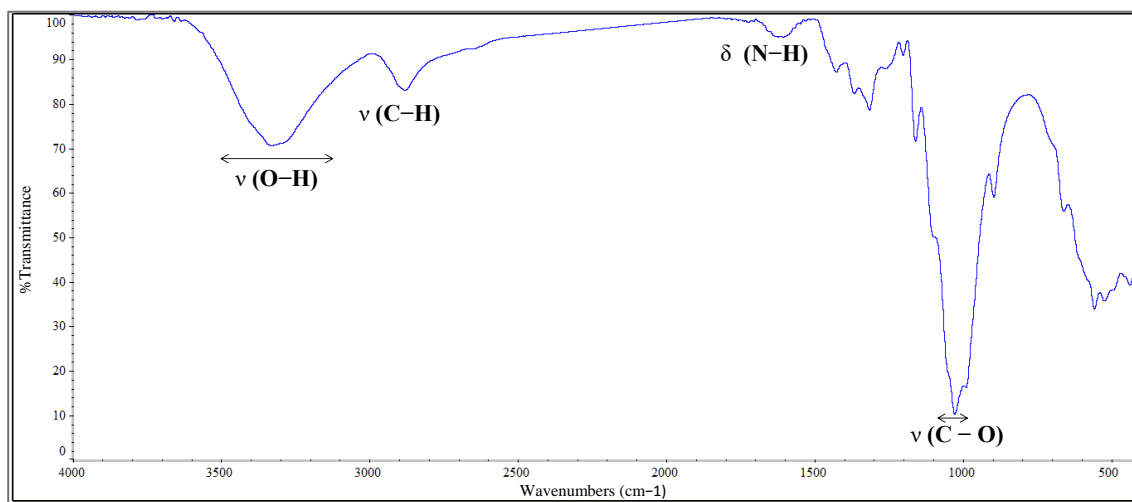


Figure 17. FTIR-ATR spectrum of K-APTES

6.3.3. K-CCFCPG Bioadsorbent

The FTIR-ATR spectrum of K-CMC (Figure 18A) shows peaks at around 3300 cm^{-1} is attributed to the O-H obtain during the etherification reaction. Also, a characteristic peak at 1700 cm^{-1} has been assigned to C-O for the ester group of the CMC products and at 1016 cm^{-1} the C-O bond of ether in glucose units.⁷⁹ The Figure 18B shows peaks at 1586 and 1411 cm^{-1} , which can be ascribed to the stretching vibrations of COO⁻ asymmetric and symmetric respectively. Also, the spectrum shows a peak at 1051 cm^{-1} , which is due to stretching vibrations of C-O, and the band at 2921 and 2874 cm^{-1} which can be assigned to C-H stretching asymmetric and symmetric vibrations because of the introduction of a large amount of CH₂ by bPEI.⁸⁰

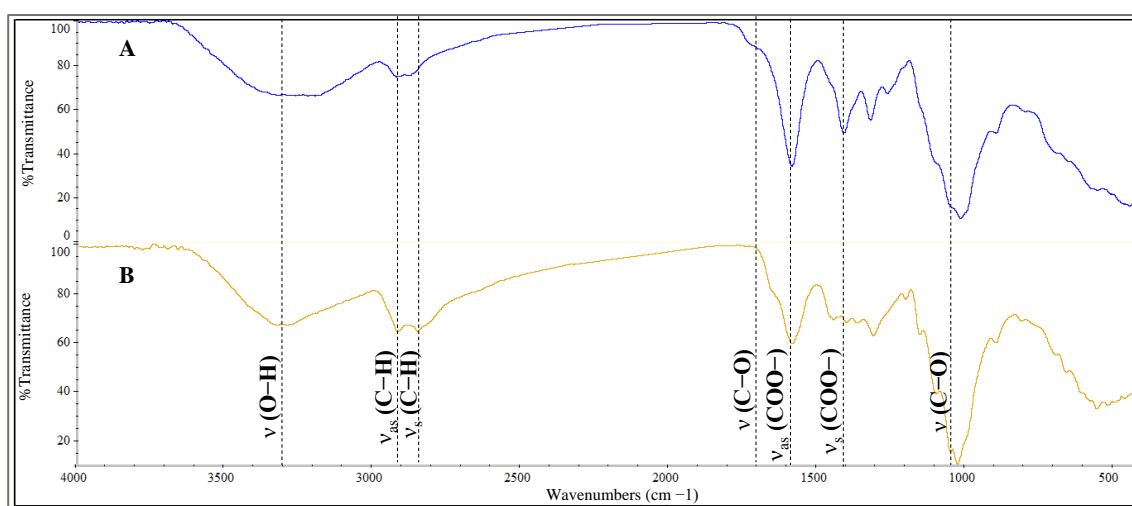


Figure 18. FTIR-ATR spectra (A) K-CMC bioadsorbent and (B) K-CCFCPG bioadsorbent

6.3.4. K-AFCPG Bioadsorbent

Figure 19 shows the spectra of K-APTES, K-FCPG and K-AFCPG in order to compare the signals that appear in each of the modifications. In the case of K-APTES with bPEI, the FTIR-ATR spectrum of K-AFCPG shows the band from 3450 to 3100 cm^{-1} is slightly less intense than K-APTES which could be assigned to the superposition of the stretching vibrations of O-H and N-H groups of amino groups of bPEI. Also, the bands at 2932 cm^{-1} and 2853 cm^{-1} are wider and more intense assigned to the symmetrical and asymmetrical C-H stretching vibrations, respectively⁸¹. In addition, a new peak appears in 1654 cm^{-1} that is attributed to C=N and at 1437 cm^{-1} can be attributed to the N-H bending vibration the terminal amine of bPEI.⁷⁴

The peak in 1101 cm^{-1} has shifted to 1053 cm^{-1} this signal is stronger and is related to the Si-O-Si bond. Comparing K-AFCPG and K-FCPG, the K-AFCPG not show new peaks. However, the bands at 2950 cm^{-1} and 2775 cm^{-1} , the peaks at $1654, 1562, 1437, 1101, 1053,$ and 1029 cm^{-1} show high intensity than K-FCPG.

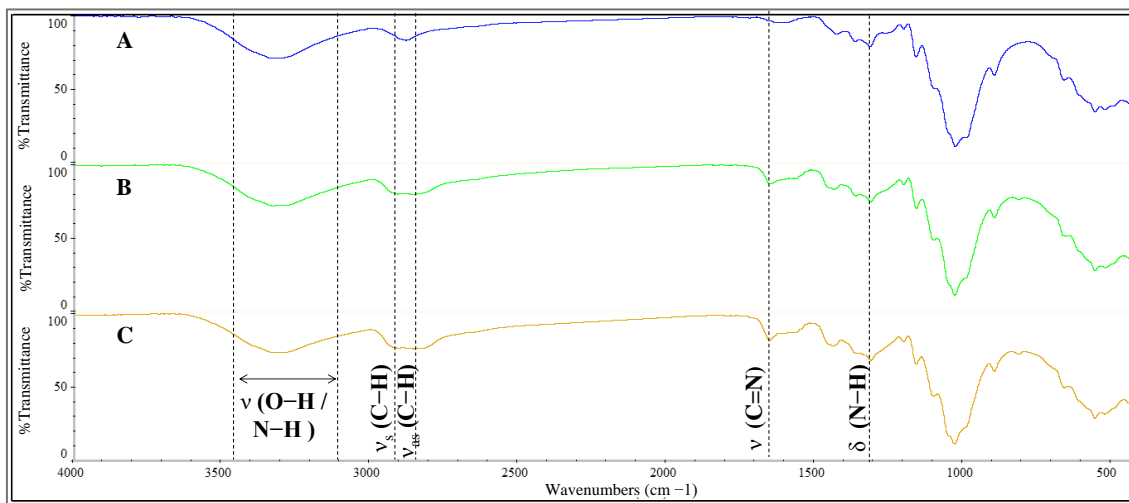


Figure 19. FTIR-ATR spectra (A) K-APTES (B) K-FCPG bioadsorbent and (C) K-AFCPG bioadsorbent

The FTIR-ATR was used to identify amine groups of bPEI, the hydroxyl groups, ether, alcohols, imine groups present on K-FCPG, K-APTES, K-CCFCPG, and K-AFCPG biomaterials.

6.4. SEM-EDS Analysis

SEM was used to observe the surface morphology of the synthesized materials. Also, the energy-dispersive X-ray spectroscopy (EDS) method was conducted to study the presence of different elements in the surface to evaluate the adequate modification. The effect of the various chemical treatments was assessed using a comparison of the materials.⁸² The SEM revealed a non-homogeneous topography for K-AFCPG, K-FCPG and K-CCFCPG, where crowds and fibrils could be identified on the surface.

The grafted bPEI-APTES molecules partially occupied the space between the cellulose molecules. However, these molecules have not damaged the cellulose structure when grafted.⁸³ SEM images show the chemical structure of cellulose microfibril has been changed small fibers as see in Figure 20 Also, Figure 21 shows a great amount of agglomerations on the surface as shown in Figure 22, rather than microfibrils smooth due to, during modification the microfibrils have swelled.⁸⁴

Additionally, K-FCPG showed a pronounced crosslinking effect Figure 21 on the surface of the modified microfibrils due to the multiple reactions of ether bond formation. Therefore, SEM micrographs helped to understand the effects of all the modifications in the morphology of the surface.⁸⁵ Furthermore, EDS allowed a mapping in the materials modified to know the elements that are present ad confirm the structure changes. This mapping shows the presence of C, O, and N atoms on the surface of the materials, as shown in section B of Figure 20, Figure 21, and Figure 22. These results confirm that amino groups and hydroxyl groups are involved in functionalized cellulose.

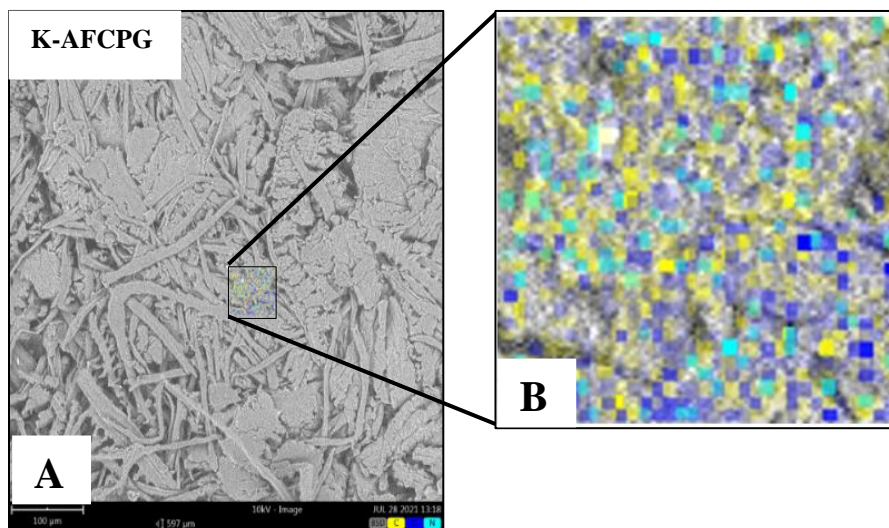


Figure 22. (A) SEM/EDS and (B) map of K-AFCPG

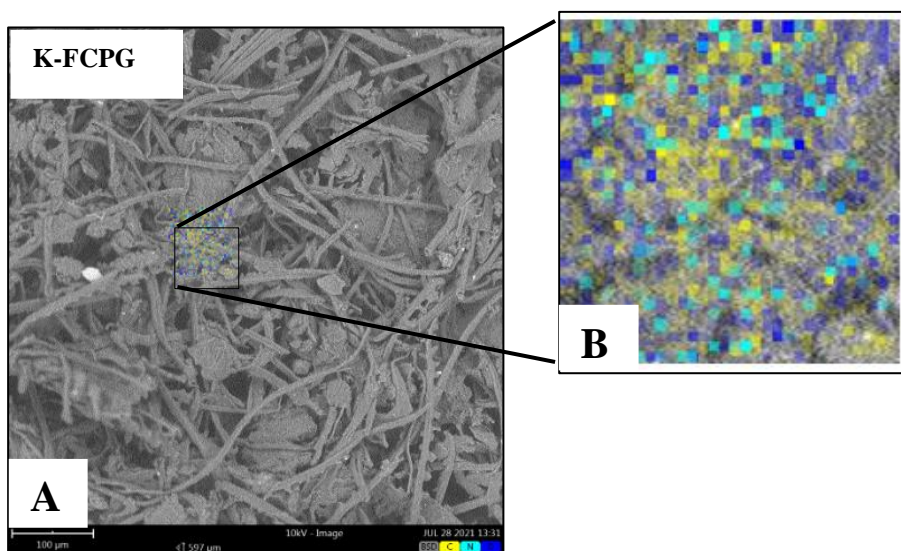


Figure 21. (A) SEM/EDS and (B) map of K-FCPG

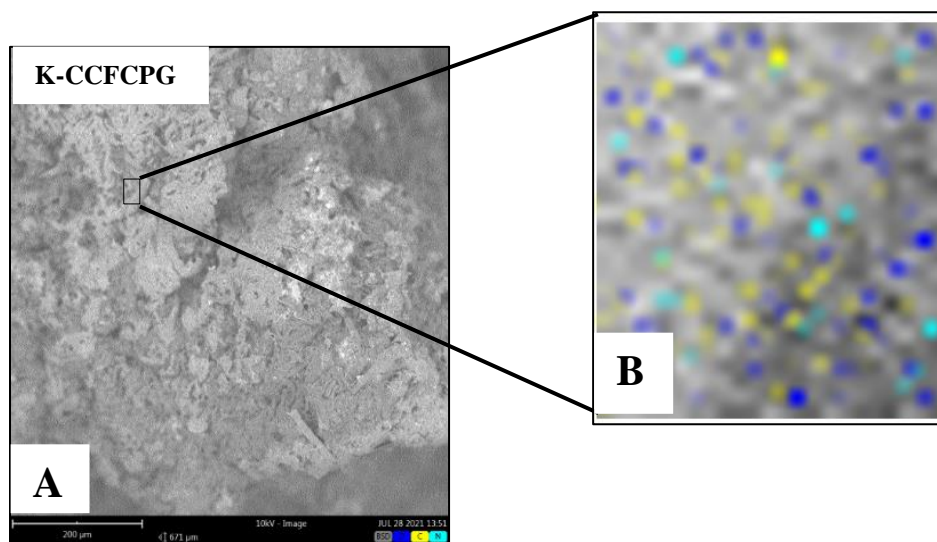


Figure 20. (A) SEM/EDS and (B) map of K-CCFCPG

6.5. Adsorption Kinetics

6.5.1. Kinetic Batch Studies on Cr (VI) Adsorption

Four experiments were prepared to vary the weight of the bioadsorbent between 5, 10, 15, and 20 mg in 5 mL of a 100 mg/L Cr solution. For about 5 h (300 min) approximately, the absorbance was taken at 352 nm, which is the absorption wavelength of Cr.

First of all, the adsorption efficiency was analyzed between K-PGG, K-AGG, and K-CCFCPG. According to Table 6, it was observed that after 204 min, K-PGG had removed 76 % while K-AGG has adsorbed 57 % and K-CCFCPG 38 % of Cr in solution. In other words, K-CCFCPG is not a potential bioadsorbent.

Second of all, evaluate the absorbance percentage between K-AGG and K-PGG and K-FCPG and K-AFCPG to compare if there was any difference in absorbance when the crosslinker was added differently. Table 6 shows the absorbance percentages of K-PGG and K-AGG and K-FCPG and K-AFCPG at different bioadsorbent ratios. K-FCPG has an average Cr adsorption of 86 % and K-AFCPG 88 %, while K-PGG has average adsorption of 71 % and K-AGG 76 %. In other words, there is a difference in the percentage of adsorption when change the way of adding GA. It also indicates that K-FCPG and K-AFCPG have better adsorption capacity when the crosslinker is added abruptly.

Lastly, the adsorption efficiency between K-FCPG and K-AFCPG was compared by varying the amount of bioadsorbent in an approximate time range from 200 min to 280 min. K-FCPG and K-AFCPG show a similar adsorption tendency since they have an adsorption percentage between 83% and 91% in approximately 250 min. finding that bioadsorbents have a similar adsorption capacity.

Table 6. Percentage of Cr (VI) adsorption with different weights of bioadsorbents

Time (min)	K-FCPG	K-AFCPG	K-PGG	K-AGG	K-CCFCPG
278	5 mg				
	86%	86%	64%	78%	-
263	10 mg				
	83%	90%	82%	68%	-
204	15 mg				
	-	-	76%	57%	38%
235	20 mg				
	91%	87%	67%	82%	-

Figure 23 shows the relationship between the percentage of adsorption and time for K-FCPG and K-AFCPG. As seen in Figure 23 K-AFCPG shows a similar adsorption trend for 5 and 20 mg. Figure 23.A there is no difference between K-FCPG and K-AFCPG, both have the same behavior. However, Figure 23.B show that K-AFCPG reaches equilibrium in less time and adsorbs faster than K-FCPG. Despite this difference, after 140 min, the two-reach equilibrium, showing that as the amount of adsorbent increases, the adsorption time decreases.

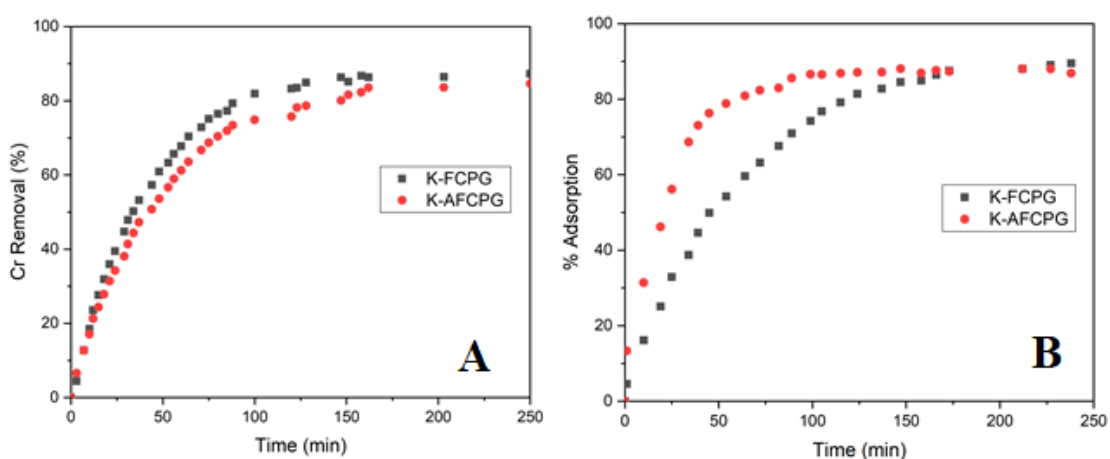


Figure 23. Cr Removal (%) of Cr (VI) (A) 5 mg and (B) 20 mg of K-FCPG and K-AFCPG

6.5.2. Cr (VI) Adsorption Kinetics of K-FCPG and K-AFCPG

The kinetic study was carried out with 5 mg of K-AFCPG and K-FCPG because 10 and 20 mg do not exhibit saturation. The Cr (VI) adsorption kinetics is shown in Figure 24 (A and B).

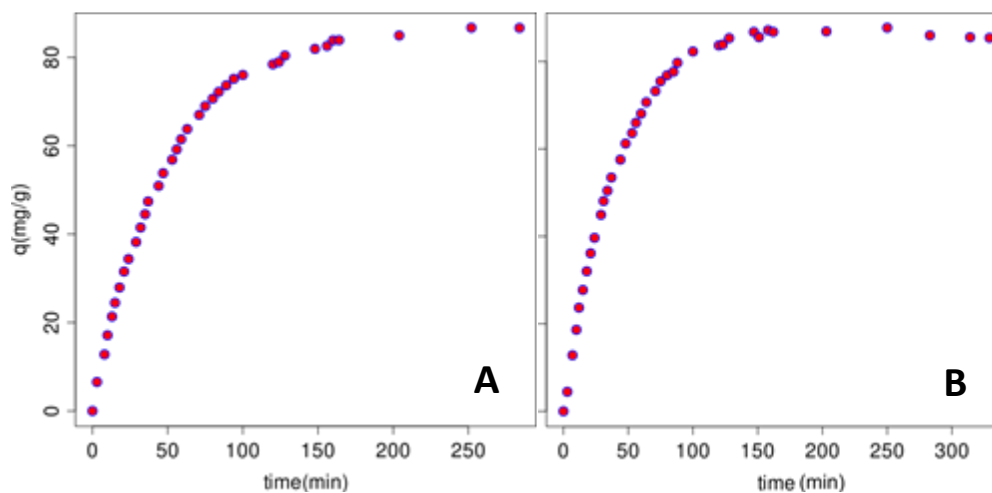


Figure 24. Cr (VI) adsorption kinetics for 100 ppm solutions in contact with 5 mg of (A) K-AFCPG and (B) K-FCPG material

The Cr (VI) adsorption on K-AFCPG and K-FCPG exhibited a saturation behavior after a contact time of about 240 and 150 min, respectively. At these times not enough adsorption sites for anionic Cr (VI) species are available in each solid. Cr (VI) adsorption kinetics of K-AFCPG and K-FCPG are similar to each other in its trend, they exhibited an adsorption behavior with their q_e values over 80.0% when 5 mg of solid is allows to has contact to a 100 ppm Cr (VI) solution. All the data was analyzed by solving the kinetic models through a script written in R. To evaluate the performance of the kinetic models, the residual standard error, RSE were calculated and compared, and residual graphs were plot and analyzed. The best fit of data was obtained using the integrated form of the pseudo-first-order model (PFO), Furusawa & Smith model (F&S), and Boyd'd external diffusion models (BED). Non-linear regression using a Gauss-Newton algorithm was applied. In Figure 25 best fits to data obtained assuming pseudo first-order adsorption for the kinetics of Cr (VI) 100 ppm and 5 mg of A) K-AFCPG, and B) K-FCPG material were shown. F&S and BED models have a quite similar curve.

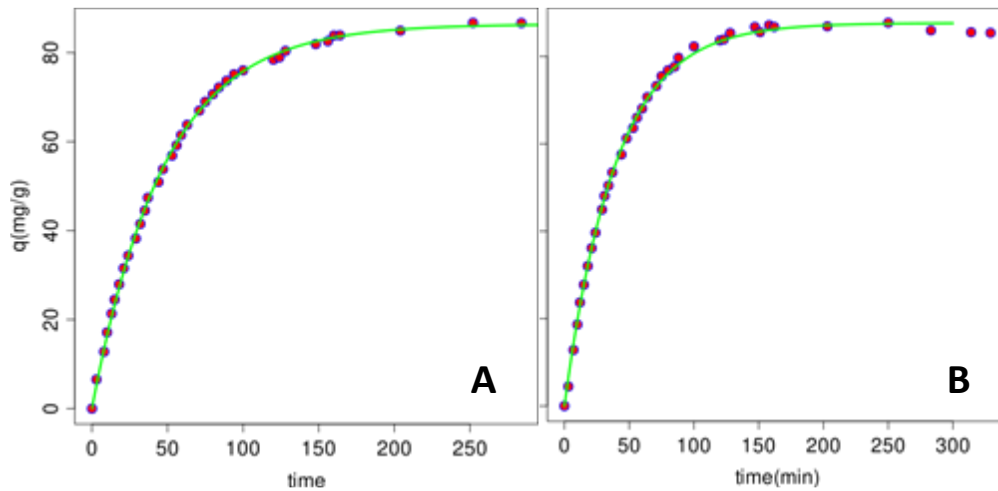


Figure 25. Cr (VI) adsorption kinetics for 100 ppm solutions in contact with 5 mg of A) K-AFCPG, and B) K-FCPG material and best fits to data were successfully obtained assuming pseudo first-order and non-linear fits

In Table 7 show the summarizes of the kinetic parameters of Cr (VI) adsorption on K-AFCPG and K-FCPG bioadsorbents.

Table 7. Kinetic parameters

Material	Pseudo First Order				Frusawa & Smith			Boyd's External Diffusion		
	$q_{e,exp}$	$q_{e,fit}$	$k_1 \times 10^{-2}$	RSE	K	$k_{F\&S} S \times 10^{-4}$	RSE	q_{∞}	$R \times 10^{-4}$	RSE
K-AFCPG	86.7	86.4 ± 0.3	2.10 ± 0.02	2.28 2	6.2 ± 0.1	181 ± 1	0.712	86.4 ± 0.3	-210 ± 2	0.717
K-FCPG	87.7	87.6 ± 0.3	2.53 ± 0.03	0.99 3	6.9 ± 0.2	221 ± 2	0.993	87.6 ± 0.3	253 ± 3	0.993

Assuming that the concentration gradient is linear, we can obtain a simplified version of Boyd's external diffusion equation, which is quite similar with the PFO model, that explain why the results are the same for both models. The F&S model assumes that, when the intraparticle diffusion is negligible, and the isotherm is linear, the external diffusion is the slowest step. Therefore, the three models seem to indicate that the process is controlled by external diffusion. The $k_{F\&S} S$ values obtained were 0.0181 and 0.0221 s⁻¹ for K-AFCPG and K-FCPG respectively. These values indicate that the velocity of K-AFCPG and K-FCPG transport from the liquid phase to solid phase is rapid enough to suggest the use of this adsorbent for the treatment of water enriched with Cr (VI).⁸⁶

Figure 26 show isotherm obtained for K-AFCPG. The isotherm is linear, supporting and validating the assumptions made in F&S models.

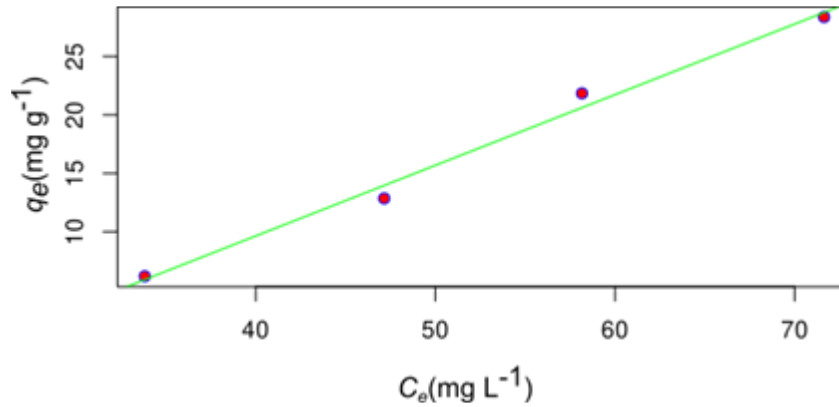


Figure 26. Isotherm for K-AFCPG

Figure 27 illustrates the adsorption mechanisms assumed by the linear model, displaying the condition when the coverage ratio of the adsorption sites is low. Therefore, the linear model can represent the monolayer adsorption at low initial adsorbate concentrations C_0 .

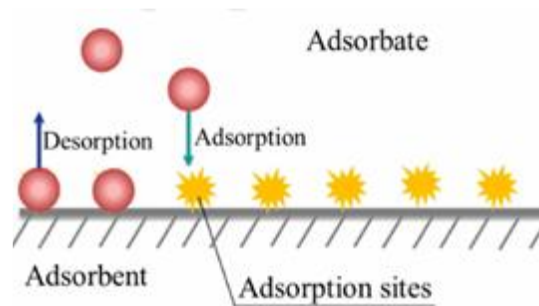


Figure 27. Adsorption mechanisms

6.6. Chromium Adsorption

6.6.1. FTIR-ATR Analysis

Figure 28 and Figure 29 show FTIR-ATR spectra of K-FCPG and K-AFCPG respectively. The first part of each figure shows the materials previous to the adsorption process and the B part of each figure evidence the Cr signals after adsorption process. Figure 30 exhibits the FTIR-ATR spectra K-FCPG and K-AFCPG loaded of Cr (VI). After adsorption of Cr (VI), the adsorption peaks at 3226 cm^{-1} and 1312 cm^{-1} related to the vibrations of hydroxyl groups are weak, while the absorption band at 1632 cm^{-1} assigned to C=N stretching of forming Schiff's base and peak at 1562 cm^{-1} associated with the N-H bonds are strong. Also, the peaks of the bands in 1100 , 1053 and 1030 cm^{-1} are involved a strong C-O stretching of COH/C-O-C pyranose ring skeletal vibration and at 612 cm^{-1} disappears. A new peaks appears at 931 , 766 and at 486 cm^{-1} characteristic peaks of Cr (VI).⁸⁷ The FTIR-ATR signals confirm that bioadsorbents adsorbed the Cr (VI). Its means that the bioadsorbents were efficient with adsorption. The results obtained by FTIR – ATR, show that adsorbent material maintains its structure despite the fact that with the presence of adsorbed Cr (VI) the chemical environment of the material changes.

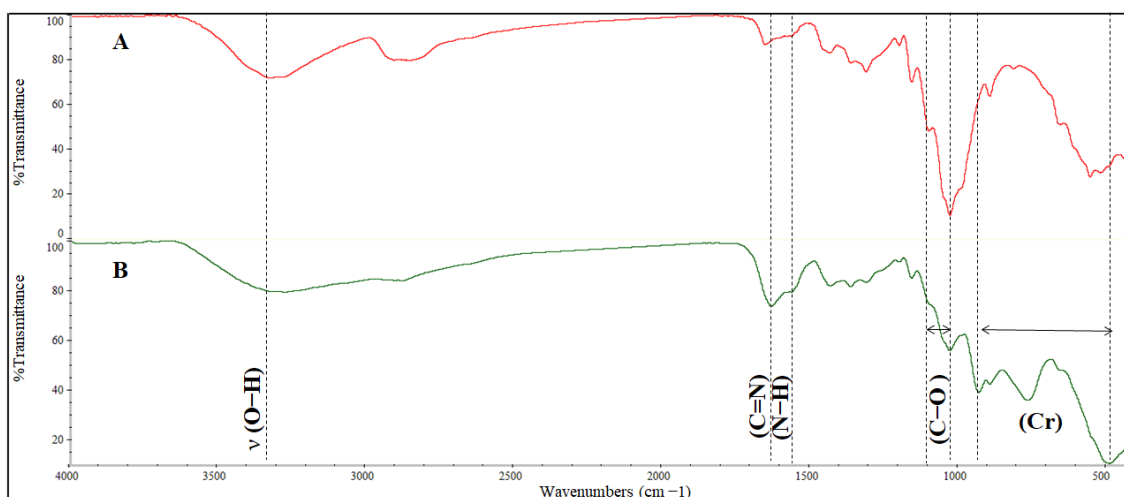


Figure 28. FTIR-ATR spectra of a) K-FCPG bioadsorbent b) K-FCPG loaded of Cr (VI)

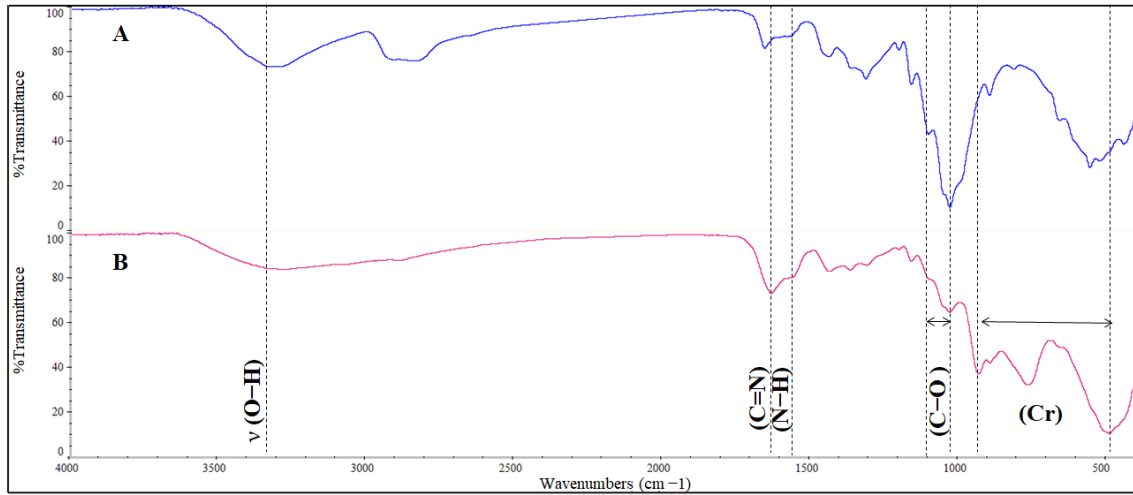


Figure 29. FTIR-ATR spectra of a) K-AFCPG bioadsorbent b) K-AFCPG loaded of Cr (VI)

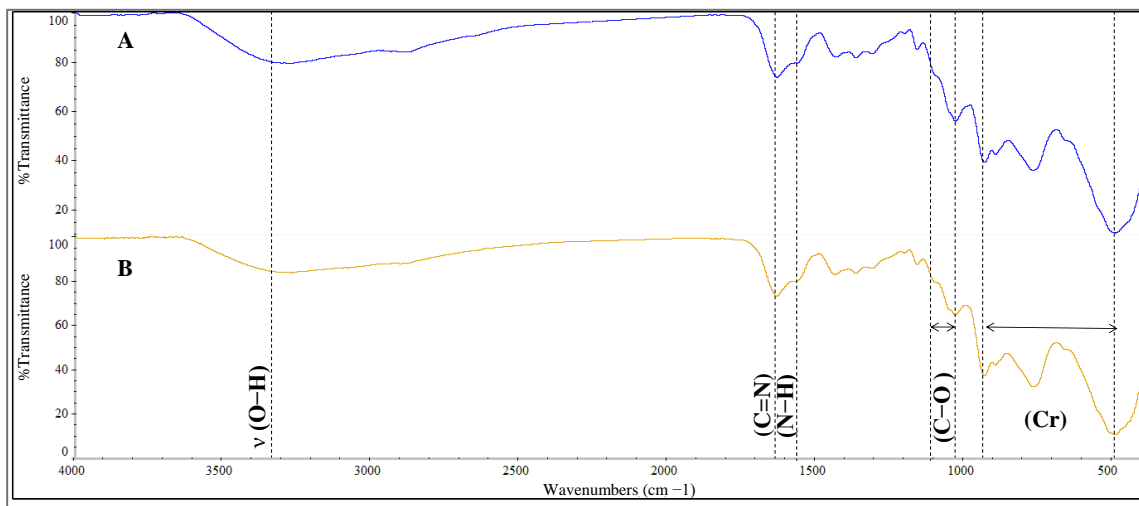


Figure 30. FTIR-ATR spectra of a) K-FCPG loaded of Cr (VI) b) K-AFCPG loaded of Cr (VI)

6.6.2. XPS Analysis

The K-FCPG and K-AFCPG were saturated with Cr (VI). During the adsorption, the materials change from pink to dark color, as shown in Figure 31. High-resolution XPS was used to study the surface and to better understand the chemical bonding of K-FCPG and K-AFCPG after adsorption of Cr (VI). The N1s and Cr 2p spectra of K-FCPG and K-AFCPG will be analyzed to know the composition of the surface of the materials after adsorption.



Figure 31. (A) K-FCPG and (B) K-AFCPG after adsorption of Cr (VI)

The XPS spectra of N1s and Cr 2p showed the changes to the material after adsorption and it was used to identify the changes in oxidation states of Cr. Figure 32 shows Cr 2p XPS spectra after Cr adsorption. The K-FCPG Cr 2p_{1/2} XPS spectra (Figure 32A) showed four peaks at 575.91, 576.97, 578.24, and 579.76 eV, and the XPS spectrum of K-AFCPG (Figure 32B) shows peaks at 575.67, 576.85, 578.53, and 580.14 eV which are assigned to Cr,⁸⁸ CrOH²⁺,⁸⁸ Cr (VI),⁸⁸ and Cr (VI) respectively. Furthermore, Cr 2p_{3/2} XPS spectra for K-FCPG show three peaks at 585.95, 587.52, and 589.04 eV. Also, K-AFCPG shows peaks are shown at 585.91, 587.23, and 588.58 eV corresponding to Cr (III), Cr (III),^{76,89} and Cr (VI)⁹⁰ respectively for each bioadsorbent.

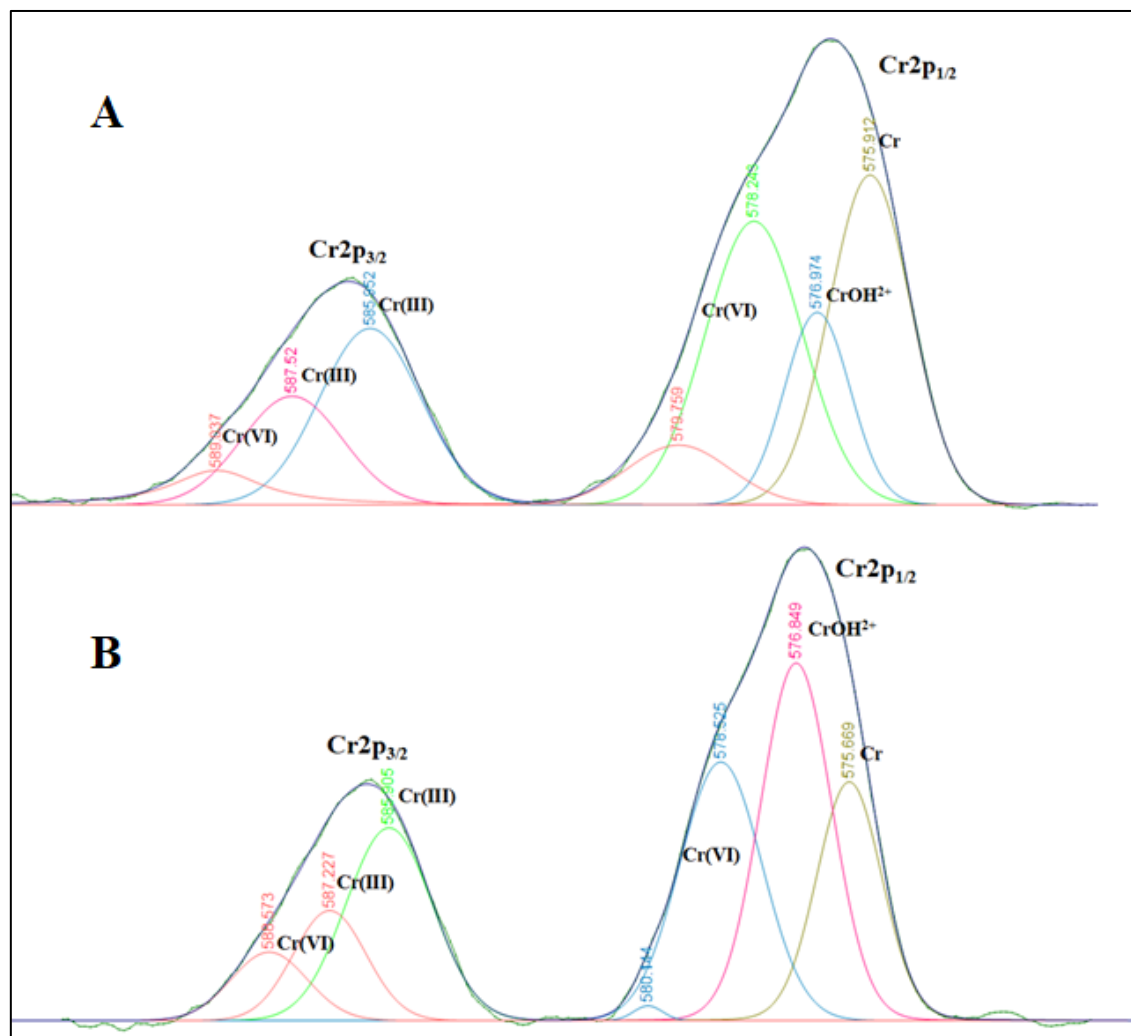


Figure 32. Cr 2p XPS spectrum of (A) K-FCPG and (B) K-AFCPG

Figure 33 shows the N1s spectra of K-FCPG and K-AFCPG after Cr (VI) adsorption. Figure 33A shows peaks at 398.66, 399.76 and 401.31 eV for K-FCPG. In the case of K-AFCPG (Figure 33B) the N1s spectrum show three peaks at 398.65, 399.74 and 401.11 eV corresponding to of the nitrogen atoms in imine ($C=N-C$),⁹¹ amine structure ($NH_2/-NH-$)⁹¹ and N^+ atom in $C=(NH^+)-C$ ⁹², respectively. The presence of $=N^+$ favors the electrostatic interaction to reduce Cr (VI).^{93,94} Also, Cr^{3+} and $CrOH^{2+}$ are adsorbed on oxidized N by covalent bonding. At the same time, the ions of Cr (VI) were adsorbed on NH^{3+} by hydrogen bonding. The XPS spectra clearly show that the bioadsorbents have successfully captured Cr in solution. Furthermore, the Cr 2p spectra show that Cr (VI) has been reduced to Cr (III), that is to say, that a redox reaction occurs on the bioadsorbent. Furthermore, the N1s spectra show the interaction mechanism between Cr (VI) and the amine groups of the bioadsorbent.⁹³

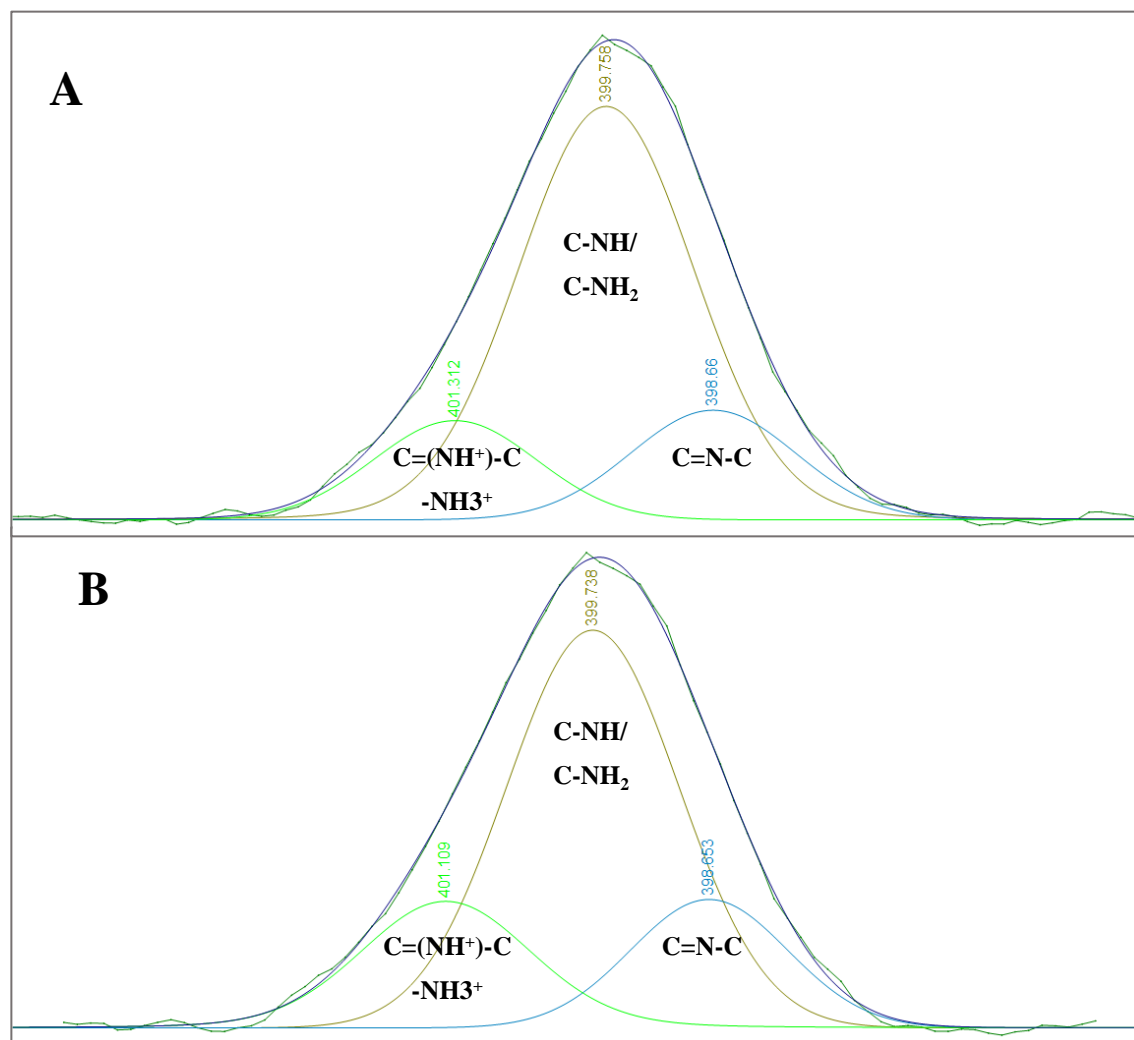


Figure 33. N1s XPS spectrum of (A) K-FCPG and (B) K-AFCPG

6.7. Proposals for Reactions of the Synthesis of Bioadsorbents Cellulose Base

After the FTIR–ATR, SEM–EDS, and XPS analyzes, reactions can be proposed for the synthesis of K-FCPG and K-AFCPG. Figure 34 shows the mechanism of K-FCPG formation. In this synthesis, cellulose, bPEI and GA were used as crosslinking agents, resulting in the formation of a Schiff's base and a hemiacetal.^{43,91} The ether bond was formed according to aldolization between the aldehyde group of GA and the C6 hydroxyl group of cellulose.⁹¹ On the other hand, the positively charged end of the GA reacts with the primary amines of the PEI to form an imine bond to finally produce the cross-linked system.

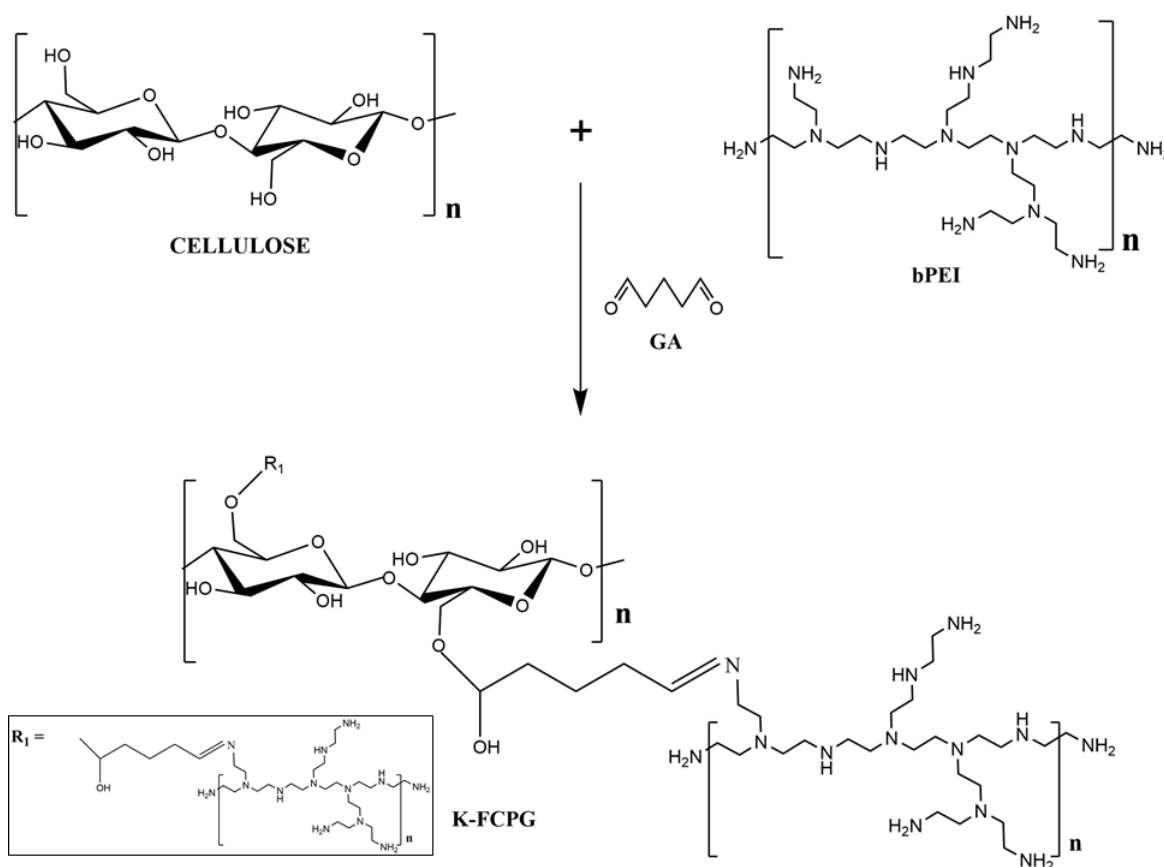


Figure 34. K-FCPG Reaction

Figure 35 shows the synthesis of K-AFCPG. This synthesis was divided into two parts, the first is the modification of the cellulose with APTES (K-APTES), and the second, the functionalization with bPEI. In the first part, performance a silylation reaction between the -OH groups of cellulose and the silanol groups of APTES⁹⁵ silanol previously obtained by hydrolysis.

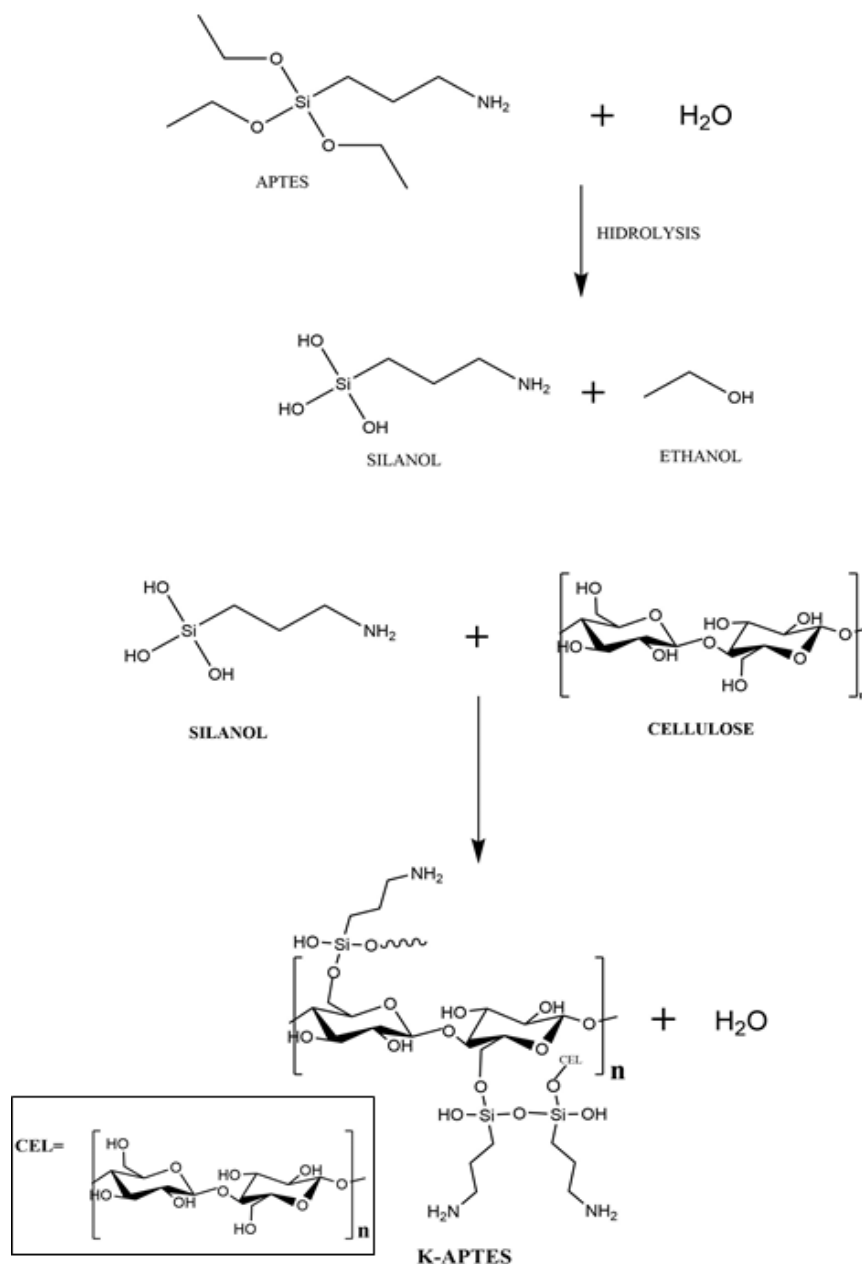


Figure 35. K-APTES reaction (a) Synthesis of Silanol and (b) Silanol and cellulose reaction

Figure 36 shows the proposed reaction between K-APTES previously prepared, bPEI, and GA as cross-linker. K-AFCPG has ether linkages formed from the OH groups of C6 of cellulose and the primary amines of bPEI. The aldehyde groups of GA were bound to the surface of K-APTES through an imine bond. Then the bPEI is linked with the rest of molecule through another imine bond to produce the cross-linked system. The amine-modified material is important for the adsorption of anion pollutants under the low pH condition. Due to the amino groups are easily protonated, thereby forming a strong electrostatic interaction between them.²⁰

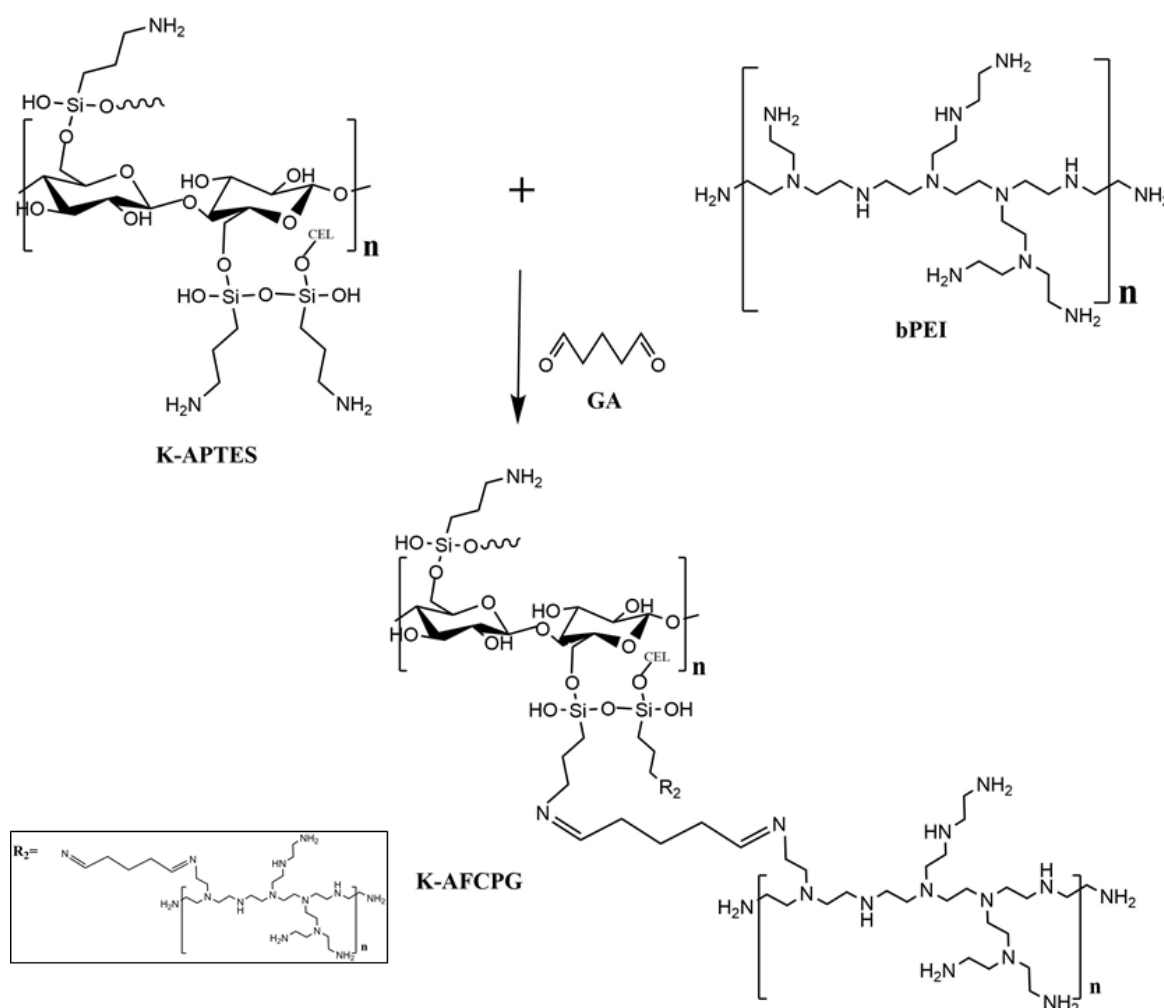


Figure 36. K-AFCPG Reaction

CHAPTER V

7. Conclusions

- Cellulose was efficiently extracted from the rice husk by alkaline treatment and a bleaching process. The percentage yield of the process was 41.7 %, and bleached cellulose presented a crystallinity index of 72.5%.
- Three environmentally-friendly composites were synthesized through cross-link reaction between the amine groups of PEI and the hydroxyl groups of cellulose using glutaraldehyde as crosslinker. Each composite was obtained through a different synthesis route, (1) direct cross linking of PEI and cellulose through glutaraldehyde (K-FCPG), (2) first carboxymethylation followed by cross linking of PEI and cellulose through glutaraldehyde (K-CCFCPG), and (3) first amine-functionalization by APTES followed by cross linking of PEI and cellulose through glutaraldehyde (K-AFCPG). The last one route has not been previously reported. The presence of imine, amine and carboxyl groups in the composites was confirmed by SEM/EDS and FTIR-ATR
- Experimental adsorption results show that K-FCPG and K-AFCPG composites have higher Cr (VI) adsorption capacities, 82 and 91% respectively.
- Kinetic data was best fit using the integrated form of the pseudo-first-order model (PFO), the Furusawa & Smith model (F&S), and the Boyd'd external diffusion models (BED). The three models indicate that the adsorption process is controlled by external diffusion. $k_{F&S}$ values obtained indicate that the velocity of transport from the liquid phase to the solid phase is rapid enough to suggest the use of this adsorbent for the treatment of water enriched with Cr (VI). While the equilibrium data were well described by the linear adsorption isotherm model.
- An adsorption mechanism involving interaction between amino groups and Cr (VI) was proposed. According to the results obtained, it can be said that there are two Cr (VI) adsorption mechanisms. First adsorption mechanisms are the $-C=N^+$ and $-NH_3$ groups participate in the reduction of Cr (VI) to Cr (III) and second adsorption mechanisms is NH_3^+ adsorb Cr (VI) ions that have not been reduced.

8. Recommendations

- Study of the adsorption the kinetics of at different pH values and concentrations of Cr (VI).
- Change the PEI and GA proportions to analyze the changes they present.
- Evaluate the adsorption capacity of CO₂.
- Perform desorption experiments.
- Evaluate the adsorption capacity of other heavy metals.
- Study of the adsorption the kinetics of at different temperatures.

9. References

- (1) Shen, M.; Zeng, Z.; Li, L.; Song, B.; Zhou, C.; Zeng, G.; Zhang, Y.; Xiao, R. Microplastics Act as an Important Protective Umbrella for Bacteria during Water / Wastewater Disinfection. *J. Clean. Prod.* **2021**, *315* (July), 128188. <https://doi.org/10.1016/j.jclepro.2021.128188>.
- (2) Musarurwa, H.; Tavengwa, N. T. Application of Carboxymethyl Polysaccharides as Bio-Sorbents for the Sequestration of Heavy Metals in Aquatic Environments. *Carbohydr. Polym.* **2020**, *237* (March), 116142. <https://doi.org/10.1016/j.carbpol.2020.116142>.
- (3) Yang, J.; Hou, B.; Wang, J.; Tian, B.; Bi, J.; Wang, N.; Li, X. Nanomaterials for the Removal of Heavy Metals from Wastewater. **2019**. <https://doi.org/10.3390/nano9030424>.
- (4) Zeitoun, M. M.; Mehana, E. S. E. Impact of Water Pollution with Heavy Metals on Fish Health: Overview and Updates. *Glob. Vet.* **2014**, *12* (2), 219–231. <https://doi.org/10.5829/idosi.gv.2014.12.02.82219>.
- (5) Masindi, V.; Muedi, K. L. Environmental Contamination by Heavy Metals. **2018**. <https://doi.org/10.5772/intechopen.76082>.
- (6) Singh, B. *Rice Husk Ash*; Elsevier Ltd, 2018. <https://doi.org/10.1016/B978-0-08-102156-9.00013-4>.
- (7) Jiang, Y.; Liu, Z.; Zeng, G.; Liu, Y.; Shao, B.; Li, Z.; Liu, Y. Polyaniline-Based Adsorbents for Removal of Hexavalent Chromium from Aqueous Solution : A Mini Review. *Environ. Sci. Pollut. Res.* **2018**. <https://doi.org/10.1007/s11356-017-1188-3>.
- (8) Vaiopoulou, E.; Gikas, P. Regulations for Chromium Emissions to the Aquatic Environment in Europe and Elsewhere. *Chemosphere* **2020**, *254*, 126876. <https://doi.org/10.1016/j.chemosphere.2020.126876>.
- (9) Cipriani-Avila, I.; Molinero, J.; Jara-Negrete, E.; Barrado, M.; Arcos, C.; Mafla, S.; Custode, F.; Vilaña, G.; Carpintero, N.; Ochoa-Herrera, V. Heavy Metal Assessment in Drinking Waters of Ecuador: Quito, Ibarra and Guayaquil. *J. Water Health* **2020**, *18* (6), 1050–1064. <https://doi.org/10.2166/wh.2020.093>.

- (10) Xining, S.; Jingjing, M.; Zengqiang, Z.; Zhiyong, Z. Biosorption of Hexavalent Chromium from Aqueous Medium with the Antibiotic Residue. *Adv. J. Food Sci. Technol.* **2015**, *7* (2), 120–128. <https://doi.org/10.19026/ajfst.7.1279>.
- (11) Singh, N. B.; Nagpal, G.; Agrawal, S. Water Purification by Using Adsorbents : A Review. *Environ. Technol. Innov.* **2018**. <https://doi.org/10.1016/j.eti.2018.05.006>.
- (12) Zhang, K.; Dai, Z.; Zhang, W.; Gao, Q.; Dai, Y.; Xia, F.; Zhang, X. EDTA-Based Adsorbents for the Removal of Metal Ions in Wastewater. *Coord. Chem. Rev.* **2021**, *434*, 213809. <https://doi.org/10.1016/j.ccr.2021.213809>.
- (13) Moon, R. J.; Martini, A.; Nairn, J.; Simonsen, J.; Youngblood, J. *Cellulose Nanomaterials Review: Structure, Properties and Nanocomposites*; 2011; Vol. 40. <https://doi.org/10.1039/c0cs00108b>.
- (14) Xu, Q.; Chen, C.; Rosswurm, K.; Yao, T.; Janaswamy, S. A Facile Route to Prepare Cellulose-Based Films. *Carbohydr. Polym.* **2016**, *149*, 274–281. <https://doi.org/10.1016/j.carbpol.2016.04.114>.
- (15) Hokkanen, S.; Bhatnagar, A.; Sillanpää, M. A Review on Modification Methods to Cellulose-Based Adsorbents to Improve Adsorption Capacity. *Water Res.* **2016**, *91*, 156–173. <https://doi.org/10.1016/j.watres.2016.01.008>.
- (16) Mahmud, M. M.; Perveen, A.; Jahan, R. A.; Matin, M. A.; Wong, S. Y.; Li, X.; Arafat, M. T. Preparation of Different Polymorphs of Cellulose from Different Acid Hydrolysis Medium. *Int. J. Biol. Macromol.* **2019**, *130*, 969–976. <https://doi.org/10.1016/j.ijbiomac.2019.03.027>.
- (17) Jordan, J. H.; Easson, M. W.; Dien, B.; Thompson, S.; Condon, B. D. Extraction and Characterization of Nanocellulose Crystals from Cotton Gin Motes and Cotton Gin Waste. *Cellulose* **2019**, *26* (10), 5959–5979. <https://doi.org/10.1007/s10570-019-02533-7>.
- (18) Julie Chandra, C. .; George, N.; Narayanankutty, S. K. Isolation and Characterization of Cellulose Nanofibrils From Arecanut Husk Fibre. *Carbohydr. Polym.* **2016**. <https://doi.org/10.1016/j.carbpol.2016.01.015>.
- (19) Islam, M. N.; Rahman, F. *Production and Modification of Nanofibrillated*

- Cellulose Composites and Potential Applications*; Elsevier Ltd, 2018.
<https://doi.org/10.1016/B978-0-08-102177-4.00006-9>.
- (20) Tan, H. F.; Ooi, B. S.; Leo, C. P. Future Perspectives of Nanocellulose-Based Membrane for Water Treatment. *J. Water Process Eng.* **2020**, *37* (May), 101502. <https://doi.org/10.1016/j.jwpe.2020.101502>.
- (21) Trache, D.; Tarchoun, A. F.; Derradji, M.; Hamidon, T. S.; Masruchin, N.; Brosse, N.; Hussin, M. H. *Nanocellulose: From Fundamentals to Advanced Applications*; 2020; Vol. 8. <https://doi.org/10.3389/fchem.2020.00392>.
- (22) Manoukian, O. S.; Sardashti, N.; Health, C.; States, U. *Biomaterials for Tissue Engineering and Regenerative Medicine*; Elsevier Inc., 2018.
<https://doi.org/10.1016/B978-0-12-801238-3.64098-9>.
- (23) Mano, J. F.; Silva, G. A.; Azevedo, H. S.; Malafaya, P. B.; Sousa, R. A.; Silva, S. S.; Boesel, L. F.; Oliveira, J. M.; Santos, T. C.; Marques, A. P.; Neves, N. M.; Reis, R. L.; Interface, J. R. S. Natural Origin Biodegradable Systems in Tissue Engineering and Regenerative Medicine : Present Status and Some Moving Trends Natural Origin Biodegradable Systems in Tissue Engineering and Regenerative Medicine : Present Status and Some Moving Trends. **2007**.
<https://doi.org/10.1098/rsif.2007.0220>.
- (24) Tayeh, B. A.; Alyousef, R.; Alabduljabbar, H.; Alaskar, A. Recycling of Rice Husk Waste for a Sustainable Concrete: A Critical Review. *J. Clean. Prod.* **2021**, *312* (May), 127734. <https://doi.org/10.1016/j.jclepro.2021.127734>.
- (25) Quispe, I.; Navia, R.; Kahhat, R. Energy Potential from Rice Husk through Direct Combustion and Fast Pyrolysis: A Review. *Waste Manag.* **2017**, *59*, 200–210. <https://doi.org/10.1016/j.wasman.2016.10.001>.
- (26) CFN. Ficha Sectorial. **2020**, *1* (1), 24.
- (27) INEC- ESPAC. *Encuesta de Superficie y Producción Agropecuaria Continua (ESPAC) 2019*; 2020.
- (28) Johar, N.; Ahmad, I.; Dufresne, A. Extraction, Preparation and Characterization of Cellulose Fibres and Nanocrystals from Rice Husk. *Ind. Crops Prod.* **2012**, *37* (1), 93–99. <https://doi.org/10.1016/j.indcrop.2011.12.016>.

- (29) Zinla, D.; Gbaha, P.; Koffi, P. M. E.; Koua, B. K. Characterization of Rice, Coffee and Cocoa Crops Residues as Fuel of Thermal Power Plant in Côte d'Ivoire. *Fuel* **2021**, 283 (April 2020).
<https://doi.org/10.1016/j.fuel.2020.119250>.
- (30) Sarangi, M.; Bhattacharyya, S.; Behera, R. C. Effect of Temperature on Morphology and Phase Transformations of Nano-Crystalline Silica Obtained from Rice Husk. *Phase Transitions* **2009**, 82 (5), 377–386.
<https://doi.org/10.1080/01411590902978502>.
- (31) Hossain, S. K. S.; Mathur, L.; Roy, P. K. Rice Husk/Rice Husk Ash as an Alternative Source of Silica in Ceramics: A Review. *J. Asian Ceram. Soc.* **2018**, 6 (4), 299–313. <https://doi.org/10.1080/21870764.2018.1539210>.
- (32) Chalapud, M. C.; Herdt, M.; Nicolao, E. S.; Ruseckaite, R. A.; Ciannamea, E. M.; Stefani, P. M. Biobased Particleboards Based on Rice Husk and Soy Proteins: Effect of the Impregnation with Tung Oil on the Physical and Mechanical Behavior. *Constr. Build. Mater.* **2020**, 230, 116996.
<https://doi.org/10.1016/j.conbuildmat.2019.116996>.
- (33) O'Connell, D. W.; Birkinshaw, C.; O'Dwyer, T. F. Heavy Metal Adsorbents Prepared from the Modification of Cellulose: A Review. *Bioresour. Technol.* **99** (15), 6709–6724. <https://doi.org/10.1016/j.biortech.2008.01.036>.
- (34) Chen, X.; Cui, J.; Xu, X.; Sun, B.; Zhang, L.; Dong, W.; Chen, C.; Sun, D. Bacterial Cellulose/Attapulgitic Magnetic Composites as an Efficient Adsorbent for Heavy Metal Ions and Dye Treatment. *Carbohydr. Polym.* **2020**, 229, 115512.
<https://doi.org/10.1016/j.carbpol.2019.115512>.
- (35) Liu, P.; Borrell, P. F.; Božič, M.; Kokol, V.; Oksman, K.; Mathew, A. P. Nanocelluloses and Their Phosphorylated Derivatives for Selective Adsorption of Ag⁺, Cu²⁺ and Fe³⁺ from Industrial Effluents. *J. Hazard. Mater.* **2015**, 294, 177–185. <https://doi.org/10.1016/j.jhazmat.2015.04.001>.
- (36) Luo, X.; Yuan, J.; Liu, Y.; Liu, C.; Zhu, X.; Dai, X.; Ma, Z.; Wang, F. *Improved Solid-Phase Synthesis of Phosphorylated Cellulose Microsphere Adsorbents for Highly Effective Pb²⁺ Removal from Water: Batch and Fixed-Bed Column Performance and Adsorption Mechanism*; 2017; Vol. 5.

- <https://doi.org/10.1021/acssuschemeng.7b00472>.
- (37) Sharma, P. R.; Chattopadhyay, A.; Zhan, C.; Sharma, S. K.; Geng, L.; Hsiao, B. S. Lead Removal from Water Using Carboxycellulose Nanofibers Prepared by Nitro-Oxidation Method. *Cellulose* **2018**, *25* (3), 1961–1973. <https://doi.org/10.1007/s10570-018-1659-9>.
- (38) Cao, J.; Fei, D.; Tian, X.; Zhu, Y.; Wang, S.; Zhang, Y.; Mao, Q.; Sun, M. Novel Modified Microcrystalline Cellulose-Based Porous Material for Fast and Effective Heavy-Metal Removal from Aqueous Solution. *Cellulose* **2017**, *24* (12), 5565–5577. <https://doi.org/10.1007/s10570-017-1504-6>.
- (39) Abou-Zeid, R. E.; Dacrory, S.; Ali, K. A.; Kamel, S. Novel Method of Preparation of Tricarboxylic Cellulose Nanofiber for Efficient Removal of Heavy Metal Ions from Aqueous Solution. *Int. J. Biol. Macromol.* **2018**, *119*, 207–214. <https://doi.org/10.1016/j.ijbiomac.2018.07.127>.
- (40) Wang, J.; Liu, M.; Duan, C.; Sun, J.; Xu, Y. Preparation and Characterization of Cellulose-Based Adsorbent and Its Application in Heavy Metal Ions Removal. *Carbohydr. Polym.* **2019**, *206*, 837–843. <https://doi.org/10.1016/j.carbpol.2018.11.059>.
- (41) Park, S. H.; Shin, S. S.; Park, C. H.; Jeon, S.; Gwon, J.; Lee, S. Y.; Kim, S. J.; Kim, H. J.; Lee, J. H. Poly(Acryloyl Hydrazide)-Grafted Cellulose Nanocrystal Adsorbents with an Excellent Cr(VI) Adsorption Capacity. *J. Hazard. Mater.* **2020**, *394* (February), 122512. <https://doi.org/10.1016/j.jhazmat.2020.122512>.
- (42) Charpentier, T. V. J.; Neville, A.; Lanigan, J. L.; Barker, R.; Smith, M. J.; Richardson, T. Preparation of Magnetic Carboxymethylchitosan Nanoparticles for Adsorption of Heavy Metal Ions. *ACS Omega* **2016**, *1* (1), 77–83. <https://doi.org/10.1021/acsomega.6b00035>.
- (43) Riva, L.; Fiorati, A.; Punta, C. Synthesis and Application of Cellulose-Polyethyleneimine Composites and Nanocomposites: A Concise Review. *Materials (Basel)*. **2021**, *14* (3), 1–22. <https://doi.org/10.3390/ma14030473>.
- (44) Wang, J.; Guo, X. Adsorption Kinetic Models: Physical Meanings, Applications, and Solving Methods. *J. Hazard. Mater.* **2020**, *390* (January), 122156. <https://doi.org/10.1016/j.jhazmat.2020.122156>.

- (45) El-Khaiary, M. I.; Malash, G. F.; Ho, Y. S. On the Use of Linearized Pseudo-Second-Order Kinetic Equations for Modeling Adsorption Systems. *Desalination* **2010**, *257* (1–3), 93–101. <https://doi.org/10.1016/j.desal.2010.02.041>.
- (46) Dutta, A. *Fourier Transform Infrared Spectroscopy*; Elsevier Inc., 2017; Vol. 2. <https://doi.org/10.1016/B978-0-323-46140-5.00004-2>.
- (47) Pozo, C.; Rodríguez-Llamazares, S.; Bouza, R.; Barral, L.; Castaño, J.; Müller, N.; Restrepo, I. Study of the Structural Order of Native Starch Granules Using Combined FTIR and XRD Analysis. *J. Polym. Res.* **2018**, *25* (12). <https://doi.org/10.1007/s10965-018-1651-y>.
- (48) Lee, J. W.; Park, W. B.; Lee, J. H.; Singh, S. P.; Sohn, K. S. A Deep-Learning Technique for Phase Identification in Multiphase Inorganic Compounds Using Synthetic XRD Powder Patterns. *Nat. Commun.* **2020**, *11* (1), 1–11. <https://doi.org/10.1038/s41467-019-13749-3>.
- (49) Inkson, B. J. *Scanning Electron Microscopy (SEM) and Transmission Electron Microscopy (TEM) for Materials Characterization*; Elsevier Ltd, 2016. <https://doi.org/10.1016/B978-0-08-100040-3.00002-X>.
- (50) Mazumder, M.; Ahmed, R.; Wajahat Ali, A.; Lee, S. J. SEM and ESEM Techniques Used for Analysis of Asphalt Binder and Mixture: A State of the Art Review. *Constr. Build. Mater.* **2018**, *186*, 313–329. <https://doi.org/10.1016/j.conbuildmat.2018.07.126>.
- (51) Newbury, D. E.; Ritchie, N. W. M. Is Scanning Electron Microscopy/Energy Dispersive X-Ray Spectrometry (SEM/EDS) Quantitative? *Scanning* **2013**, *35* (3), 141–168. <https://doi.org/10.1002/sca.21041>.
- (52) Kwiecińska, B.; Pusz, S.; Valentine, B. J. Application of Electron Microscopy TEM and SEM for Analysis of Coals, Organic-Rich Shales and Carbonaceous Matter. *Int. J. Coal Geol.* **2019**, *211* (December 2018), 103203. <https://doi.org/10.1016/j.coal.2019.05.010>.
- (53) Mujahid, A.; Dickert, F. L. *Molecularly Imprinted Polymers for Sensors: Comparison of Optical and Mass-Sensitive Detection*; Elsevier B.V., 2012. <https://doi.org/10.1016/B978-0-444-56331-6.00006-2>.

- (54) Wang, H.; Chu, P. K. *Surface Characterization of Biomaterials*; Elsevier, 2013. <https://doi.org/10.1016/B978-0-12-415800-9.00004-8>.
- (55) Patel, D. I.; Roychowdhury, T.; Jain, V.; Shah, D.; Avval, T. G.; Chatterjee, S.; Bahr, S.; Dietrich, P.; Meyer, M.; Thißen, A.; Linford, M. R.; Patel, D. I.; Roychowdhury, T.; Jain, V.; Shah, D.; Avval, T. G.; Chatterjee, S.; Bahr, S.; Dietrich, P.; Meyer, M.; Thißen, A.; Linford, M. R. Characterization of Various Materials Introduction to Near-Ambient Pressure x-Ray Photoelectron Spectroscopy Characterization of Various Materials. **2019**, *016801*. <https://doi.org/10.1116/1.5109118>.
- (56) Oliveira, J. P. de; Bruni, G. P.; Lima, K. O.; Halal, S. L. M. El; Rosa, G. S. da; Dias, A. R. G.; Zavareze, E. da R. Cellulose Fibers Extracted from Rice and Oat Husks and Their Application in Hydrogel. *Food Chem.* **2017**, *221*, 153–160. <https://doi.org/10.1016/j.foodchem.2016.10.048>.
- (57) Chen, X.; Liu, L.; Luo, Z.; Shen, J.; Ni, Q.; Yao, J. Facile Preparation of a Cellulose-Based Bioadsorbent Modified by HPEI in Heterogeneous System for High-efficiency Removal of Multiple Types of Dyes. *React. Funct. Polym.* **2018**, *125* (January), 77–83. <https://doi.org/10.1016/j.reactfunctpolym.2018.02.009>.
- (58) Neves, R. M.; Ornaghi, H. L.; Zattera, A. J.; Amico, S. C. The Influence of Silane Surface Modification on Microcrystalline Cellulose Characteristics. *Carbohydr. Polym.* **2019**, *230*, 115595. <https://doi.org/10.1016/j.carbpol.2019.115595>.
- (59) Boufi, S.; Chaker, A. Easy Production of Cellulose Nanofibrils from Corn Stalk by a Conventional High Speed Blender. *Ind. Crops Prod.* **2016**, *93*, 39–47. <https://doi.org/10.1016/j.indcrop.2016.05.030>.
- (60) Shui, T.; Feng, S.; Chen, G.; Li, A.; Yuan, Z.; Shui, H.; Kuboki, T.; Xu, C. Biomass and Bioenergy Synthesis of Sodium Carboxymethyl Cellulose Using Bleached Crude Cellulose Fractionated from Cornstalk. **2017**, *105*, 51–58. <https://doi.org/10.1016/j.biombioe.2017.06.016>.
- (61) Segal, L.; Creely, J. J.; Martin, A. E.; Conrad, C. M. An Empirical Method for Estimating the Degree of Crystallinity of Native Cellulose Using the X-Ray

- Diffractionmeter. *Text. Res. J.* **1959**, 29 (10), 786–794.
<https://doi.org/10.1177/004051755902901003>.
- (62) French, A. D.; Santiago Cintrón, M. Cellulose Polymorphy, Crystallite Size, and the Segal Crystallinity Index. *Cellulose* **2013**, 20 (1), 583–588.
<https://doi.org/10.1007/s10570-012-9833-y>.
- (63) Wojdyr, M. Fityk : A General-Purpose Peak Fitting Program Fityk : A General-Purpose Peak Fitting Program. *Appl. Crystallogr.* **2010**, 1126–1128.
<https://doi.org/10.1107/S0021889810030499>.
- (64) Oliveira, J. P. de; Bruni, G. P.; Lima, K. O.; Halal, S. L. M. El; Rosa, G. S. da; Dias, A. R. G.; Zavareze, E. da R. Cellulose Fibers Extracted from Rice and Oat Husks and Their Application in Hydrogel. *Food Chem.* **2017**, 221, 153–160.
<https://doi.org/10.1016/j.foodchem.2016.10.048>.
- (65) Lakshmi, D. S.; Trivedi, N.; Reddy, C. R. K. Synthesis and Characterization of Seaweed Cellulose Derived Carboxymethyl Cellulose. *Carbohydr. Polym.* **2016**, 157, 1604–1610. <https://doi.org/10.1016/j.carbpol.2016.11.042>.
- (66) Soni, B.; Hassan, E. B.; Mahmoud, B. Chemical Isolation and Characterization of Different Cellulose Nanofibers from Cotton Stalks. *Carbohydr. Polym.* **2015**, 134, 581–589. <https://doi.org/10.1016/j.carbpol.2015.08.031>.
- (67) Li, W. Y.; Jin, A. X.; Liu, C. F.; Sun, R. C.; Zhang, A. P.; Kennedy, J. F. Homogeneous Modification of Cellulose with Succinic Anhydride in Ionic Liquid Using 4-Dimethylaminopyridine as a Catalyst. *Carbohydr. Polym.* **2009**, 78 (3), 389–395. <https://doi.org/10.1016/j.carbpol.2009.04.028>.
- (68) Arar, Ö. Preparation of Anion-Exchange Cellulose for the Removal of Chromate. *J. Chil. Chem. Soc.* **2019**, 64 (2), 4471–4474. <https://doi.org/10.4067/S0717-97072019000204471>.
- (69) Khanjanzadeh, H.; Behrooz, R.; Bahramifar, N.; Gindl-Altmutter, W.; Bacher, M.; Edler, M.; Griesser, T. Surface Chemical Functionalization of Cellulose Nanocrystals by 3-Aminopropyltriethoxysilane. *Int. J. Biol. Macromol.* **2017**, 106, 1288–1296. <https://doi.org/10.1016/j.ijbiomac.2017.08.136>.
- (70) Chen, W.; He, H.; Zhu, H.; Cheng, M.; Li, Y.; Wang, S. Thermo-Responsive

- Cellulose-Based Material with Switchable Wettability for Controllable Oil/Water Separation. *Polymers (Basel)*. **2018**, *10* (6).
<https://doi.org/10.3390/polym10060592>.
- (71) Bansal, M.; Chauhan, G. S.; Kaushik, A.; Sharma, A. Extraction and Functionalization of Bagasse Cellulose Nanofibres to Schiff-Base Based Antimicrobial Membranes. *Int. J. Biol. Macromol.* **2016**, *91*, 887–894.
<https://doi.org/10.1016/j.ijbiomac.2016.06.045>.
- (72) Campbell, S.; Bernard, F. L.; Rodrigues, D. M.; Rojas, M. F.; Carreño, L. Á.; Chaban, V. V.; Einloft, S. Performance of Metal-Functionalized Rice Husk Cellulose for CO₂ Sorption and CO₂/N₂ Separation. *Fuel* **2019**, *239* (August 2018), 737–746. <https://doi.org/10.1016/j.fuel.2018.11.078>.
- (73) Sun, X. F.; Wang, S. G.; Cheng, W.; Fan, M.; Tian, B. H.; Gao, B. Y.; Li, X. M. Enhancement of Acidic Dye Biosorption Capacity on Poly(Ethylenimine) Grafted Anaerobic Granular Sludge. *J. Hazard. Mater.* **2011**, *189* (1–2), 27–33.
<https://doi.org/10.1016/j.jhazmat.2011.01.028>.
- (74) Wang, S.; Xiao, K.; Mo, Y.; Yang, B.; Vincent, T.; Faur, C.; Guibal, E. Selenium(VI) and Copper(II) Adsorption Using Polyethyleneimine-Based Resins: Effect of Glutaraldehyde Crosslinking and Storage Condition. *J. Hazard. Mater.* **2020**, *386* (Vi), 121637. <https://doi.org/10.1016/j.jhazmat.2019.121637>.
- (75) Li, J.; Yuan, S.; Zhu, J.; Van der Bruggen, B. High-Flux, Antibacterial Composite Membranes via Polydopamine-Assisted PEI-TiO₂/Ag Modification for Dye Removal. *Chem. Eng. J.* **2019**, *373*, 275–284.
<https://doi.org/10.1016/j.cej.2019.05.048>.
- (76) Guo, D. M.; An, Q. Da; Xiao, Z. Y.; Zhai, S. R.; Shi, Z. Polyethyleneimine-Functionalized Cellulose Aerogel Beads for Efficient Dynamic Removal of Chromium(VI) from Aqueous Solution. *R. Soc. Chem. Adv.* **2017**, *7* (85), 54039–54052. <https://doi.org/10.1039/c7ra09940a>.
- (77) Zhang, X. F.; Feng, Y.; Wang, Z.; Jia, M.; Yao, J. Fabrication of Cellulose Nanofibrils/UiO-66-NH₂ Composite Membrane for CO₂/N₂ Separation. *J. Memb. Sci.* **2018**, *568*, 10–16. <https://doi.org/10.1016/j.memsci.2018.09.055>.
- (78) Song, M.; Xu, J. Preparation of Polyethyleneimine-Functionalized Graphene

- Oxide Composite and Its Application in Electrochemical Ammonia Sensors. *Electroanalysis* **2013**, 25 (2), 523–530. <https://doi.org/10.1002/elan.201200376>.
- (79) Yadollahi, M.; Namazi, H. Synthesis and Characterization of Carboxymethyl Cellulose / Layered Double Hydroxide Nanocomposites. *J. Nanoparticle Res.* **2013**. <https://doi.org/10.1007/s11051-013-1563-z>.
- (80) Song, L.; Liu, F.; Zhu, C.; Li, A. Facile One-Step Fabrication of Carboxymethyl Cellulose Based Hydrogel for Highly Efficient Removal of Cr(VI) under Mild Acidic Condition. *Chem. Eng. J.* **2019**, 369 (March), 641–651. <https://doi.org/10.1016/j.cej.2019.03.126>.
- (81) Wen, S.; Zheng, F.; Shen, M.; Shi, X. Surface Modification and PEGylation of Branched Polyethyleneimine for Improved Biocompatibility. *J. Appl. Polym. Sci.* **2013**, 3807–3813. <https://doi.org/10.1002/app.38444>.
- (82) Jokar, M.; Naeimi, H.; Nabi Bidhendi, G. Preparation and Characterization of Cellulose Sulfate/Pd Nanocatalysts with Remarkable Efficiency for Suzuki–Miyaura Reaction. *Appl. Organomet. Chem.* **2021**, 35 (8), 1–10. <https://doi.org/10.1002/aoc.6266>.
- (83) Guo, D. M.; An, Q. Da; Xiao, Z. Y.; Zhai, S. R.; Shi, Z. Polyethylenimine-Functionalized Cellulose Aerogel Beads for Efficient Dynamic Removal of Chromium(VI) from Aqueous Solution. *RSC Adv.* **2017**, 7 (85), 54039–54052. <https://doi.org/10.1039/c7ra09940a>.
- (84) Nazir, F.; Iqbal, M. Synthesis, Characterization and Cytotoxicity Studies of Aminated Microcrystalline Cellulose Derivatives against Melanoma and Breast Cancer Cell Lines. *Polymers (Basel)*. **2020**, 12 (11), 1–20. <https://doi.org/10.3390/polym12112634>.
- (85) Voicu, S. I.; Thakur, V. K. Aminopropyltriethoxysilane as a Linker for Cellulose-Based Functional Materials: New Horizons and Future Challenges. *Curr. Opin. Green Sustain. Chem.* **2021**, 30 (Figure 1), 100480. <https://doi.org/10.1016/j.cogsc.2021.100480>.
- (86) Özer, A.; Akkaya, G.; Turabik, M. The Biosorption of Acid Red 337 and Acid Blue 324 on *Enteromorpha Prolifera*: The Application of Nonlinear Regression Analysis to Dye Biosorption. *Chem. Eng. J.* **2005**, 112 (1–3), 181–190.

- <https://doi.org/10.1016/j.cej.2005.07.007>.
- (87) Trivedi, M. K.; Tallapragada, R. M.; Branton, A.; Trivedi, D.; Nayak, G.; Latiyal, O. Characterization of Physical, Thermal and Structural Properties of Chromium (VI) Oxide Powder: Impact of Biofield Treatment. **2015**, *4* (1), 1–4.
<https://doi.org/10.4172/2168-9806.1000128>.
- (88) Choi, K.; Lee, S.; Park, J. O.; Park, J.; Cho, S.; Lee, S. Y.; Lee, J. H.; Choi, J. Chromium Removal from Aqueous Solution by a PEI-Silica Nanocomposite. *Sci. Rep.* **2018**. <https://doi.org/10.1038/s41598-018-20017-9>.
- (89) Zhang, S.; Chen, H.; Zhang, S.; Kai, C.; Jiang, M.; Wang, Q.; Zhou, Z. Polyethylenimine Grafted H₂O₂-Oxidized Cellulose Membrane as a Novel Biosorbent for Cr(VI) Adsorption and Detoxification from Aqueous Solution. *Cellulose* **2019**, *26* (5), 3437–3453. <https://doi.org/10.1007/s10570-019-02325-z>.
- (90) Wang, H.; Zhang, M.; Lv, Q. Removal Efficiency and Mechanism of Cr(VI) from Aqueous Solution by Maize Straw Biochars Derived at Different Pyrolysis Temperatures. *Water (Switzerland)* **2019**, *11* (4), 5–7.
<https://doi.org/10.3390/w11040781>.
- (91) Chen, X.; Liu, L.; Luo, Z.; Shen, J.; Ni, Q.; Yao, J. Facile Preparation of a Cellulose-Based Bioadsorbent Modified by HPEI in Heterogeneous System for High-Efficiency Removal of Multiple Types of Dyes. *React. Funct. Polym.* **2018**, *125* (February), 77–83. <https://doi.org/10.1016/j.reactfunctpolym.2018.02.009>.
- (92) Mohtasebi, A.; Chowdhury, T.; Hsu, L. H. H.; Biesinger, M. C.; Kruse, P. Interfacial Charge Transfer between Phenyl-Capped Aniline Tetramer Films and Iron Oxide Surfaces. *J. Phys. Chem. C* **2016**, *120* (51), 29248–29263.
<https://doi.org/10.1021/acs.jpcc.6b09950>.
- (93) Zhu, K.; Chen, C.; Xu, H.; Gao, Y.; Tan, X.; Alsaedi, A.; Hayat, T. Cr(VI) Reduction and Immobilization by Core-Double-Shell Structured Magnetic Polydopamine@Zeolitic Imidazolate Frameworks-8 Microspheres. *ACS Sustain. Chem. Eng.* **2017**, *5* (8), 6795–6802.
<https://doi.org/10.1021/acssuschemeng.7b01036>.
- (94) Pakade, V. E.; Tavengwa, N. T.; Madikizela, L. M. Recent Advances in Hexavalent Chromium Removal from Aqueous Solutions by Adsorptive

Methods. *RSC Adv.* **2019**, *9* (45), 26142–26164.

<https://doi.org/10.1039/c9ra05188k>.

- (95) Magalhães, S.; Alves, L.; Medronho, B.; Fonseca, A. C.; Romano, A.; Coelho, J. F. J.; Norgren, M. Brief Overview on Bio-Based Adhesives and Sealants. *Polymers (Basel)*. **2019**, *11* (10). <https://doi.org/10.3390/polym11101685>.